iScience

CellPress

Article

Electron Microscopic Detection of Single Membrane Proteins by a Specific Chemical Labeling

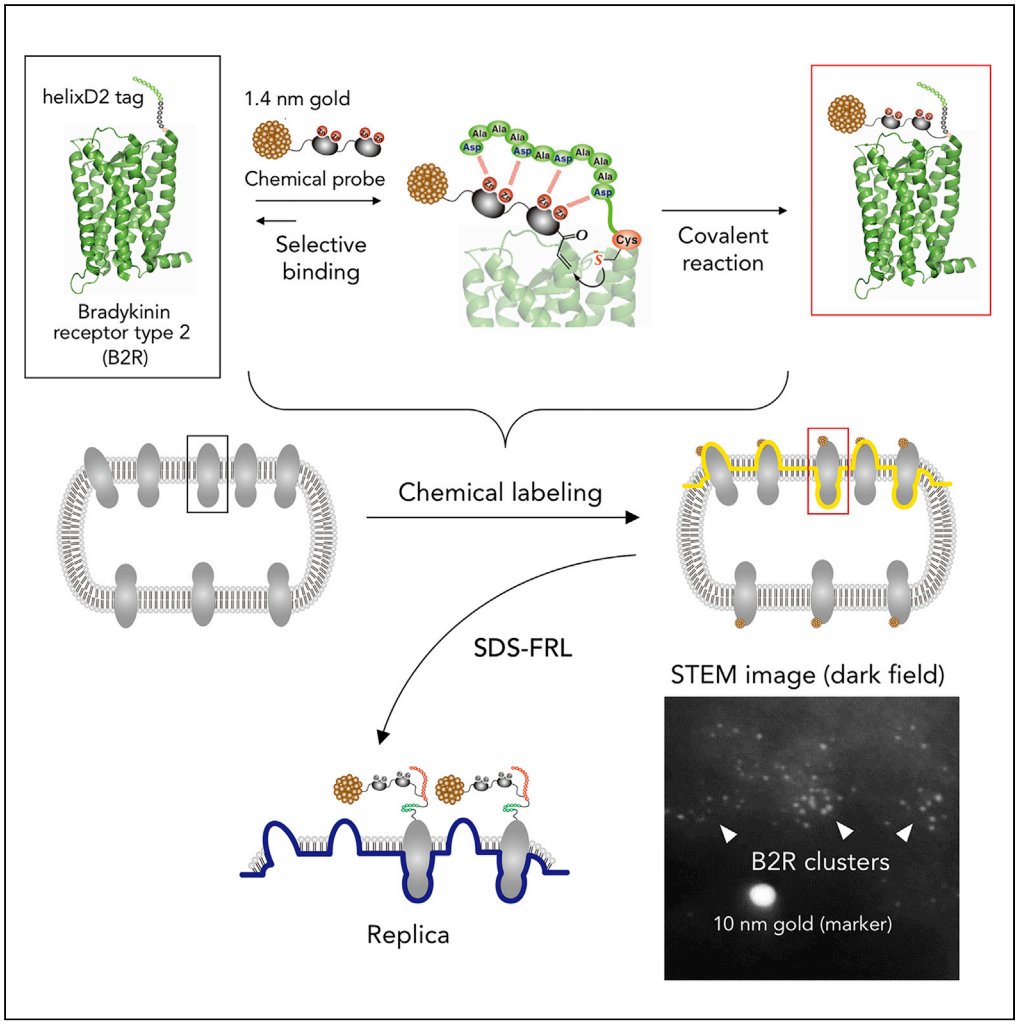

Shigekazu Tabata, Marijo Jevtic, Nobutaka Kurashige, ..., Itaru Hamachi, Ryuichi Shigemoto, Akio Ojida

ryuichi.shigemoto@ist.ac.at (R.S.)
ojida@phar.kyushu-u.ac.jp (A.O.)

HIGHLIGHTS

Developed peptide tag/probe pair enables specific chemical labeling of proteins

Chemical labeling visualizes GPCRs on cell surface with 1.4-nm gold particles

Chemical labeling has higher spatial resolution than immunogold labeling in EM

Chemical labeling shows a few times higher efficiency than immunogold labeling

Tabata et al., iScience *22*, 256–268
December 20, 2019
https://doi.org/10.1016/j.isci.2019.11.025

iScience

CellPress

Article

Electron Microscopic Detection of Single Membrane Proteins by a Specific Chemical Labeling

Shigekazu Tabata,[1,2,5] Marijo Jevtic,[2,5] Nobutaka Kurashige,[1] Hirokazu Fuchida,[1] Munetsugu Kido,[1] Kazushi Tani,[1] Naoki Zenmyo,[1] Shohei Uchinomiya,[1] Harumi Harada,[2] Makoto Itakura,[3] Itaru Hamachi,[4] Ryuichi Shigemoto,[2,*] and Akio Ojida[1,6,*]

SUMMARY

Electron microscopy (EM) is a technology that enables visualization of single proteins at a nanometer resolution. However, current protein analysis by EM mainly relies on immunolabeling with gold-particle-conjugated antibodies, which is compromised by large size of antibody, precluding precise detection of protein location in biological samples. Here, we develop a specific chemical labeling method for EM detection of proteins at single-molecular level. Rational design of α-helical peptide tag and probe structure provided a complementary reaction pair that enabled specific cysteine conjugation of the tag. The developed chemical labeling with gold-nanoparticle-conjugated probe showed significantly higher labeling efficiency and detectability of high-density clusters of tag-fused G protein-coupled receptors in freeze-fracture replicas compared with immunogold labeling. Furthermore, in ultrathin sections, the spatial resolution of the chemical labeling was significantly higher than that of antibody-mediated labeling. These results demonstrate substantial advantages of the chemical labeling approach for single protein visualization by EM.

INTRODUCTION

Electron microscopy (EM) is a powerful technique for detecting localization and distribution of a protein of interest (POI) in biological specimens at a nanometer resolution. The most common approach in EM detection of POI is immunogold labeling, in which POI is specifically labeled with a high-electron-density gold particle by using specific antibodies (Faulk and Taylor, 1971). However, immunogold labeling usually suffers from inherent problems, which are mainly associated with the large molecular size of antibody (*ca.* 150 kDa). First, the use of bulky primary and secondary antibodies locates gold particles 20–30 nm away from POI (Fijita et al., 2007), precluding precise detection of protein localization in biological samples. Second, the bulkiness of antibody limits simultaneous labeling of different components of a protein complex. Since numerous proteins function by forming permanent or transient protein complexes in living cells (Srihari et al., 2015; Havugimana et al., 2012), this limitation dramatically diminishes the utility of EM in protein analysis. Third, the large molecular size of antibody hinders its penetration into biological specimens, making it challenging to quantitatively compare POI localization along tissue depth (Masugi-Tokita and Shigemoto, 2007). Fourth, the development of an antibody that is highly selective toward POI is often technically demanding. Chemical protein labeling methods using small molecular probe could potentially overcome these problems. However, despite their extensive use in fluorescence imaging, application to single-protein detection by EM is yet to be reported.

The method for covalent labeling of proteins with a synthetic chemical probe enables functional analyses of POI under biological conditions. Various protein labeling methods have been devised over the past 20 years and mainly used for fluorescence imaging of POI under live cell conditions (Xue et al., 2015; Dean and Palmer, 2014; Krall et al., 2016). Among them, specific cysteine conjugation using reactive peptide tag-probe pair has attracted considerable attention (Schneider and Hackenberger, 2017; Lotze et al., 2016). The pioneering work of Tsien and co-workers led to the development of a method employing a genetically encoded short peptide tag (CysCysXXCysCys) and a biarsenical probe (Griffin et al., 1998). Since then, several peptide tag-based approaches, including oligohistidine tag (His6–10) (Martos-Maldonado et al., 2018; Uchinomiya et al., 2013), π-clamp (Phe-Cys-Pro-Phe) (Zhang et al., 2016), and CX10R7 tag (VTNQECCSIPM) (Ramil et al., 2016), have been devised for specific protein labeling. As a different

[1]Graduate School of Pharmaceutical Sciences, Kyushu University, Maidashi, Higashi-ku, Fukuoka, Japan

[2]Institute of Science and Technology Austria, 3400 Klosterneuburg, Austria

[3]Department of Biochemistry, Kitasato University School of Medicine, Sagamihara, Kanagawa, Japan

[4]Department of Synthetic Chemistry and Biological Chemistry, Graduate School of Engineering, Kyoto University, Katsura, Nishikyo-ku, Kyoto, Japan

[5]These authors contributed equally

[6]Lead Contact

*Correspondence: ryuichi.shigemoto@ist.ac.at (R.S.), ojida@phar.kyushu-u.ac.jp (A.O.)

https://doi.org/10.1016/j.isci.2019.11.025

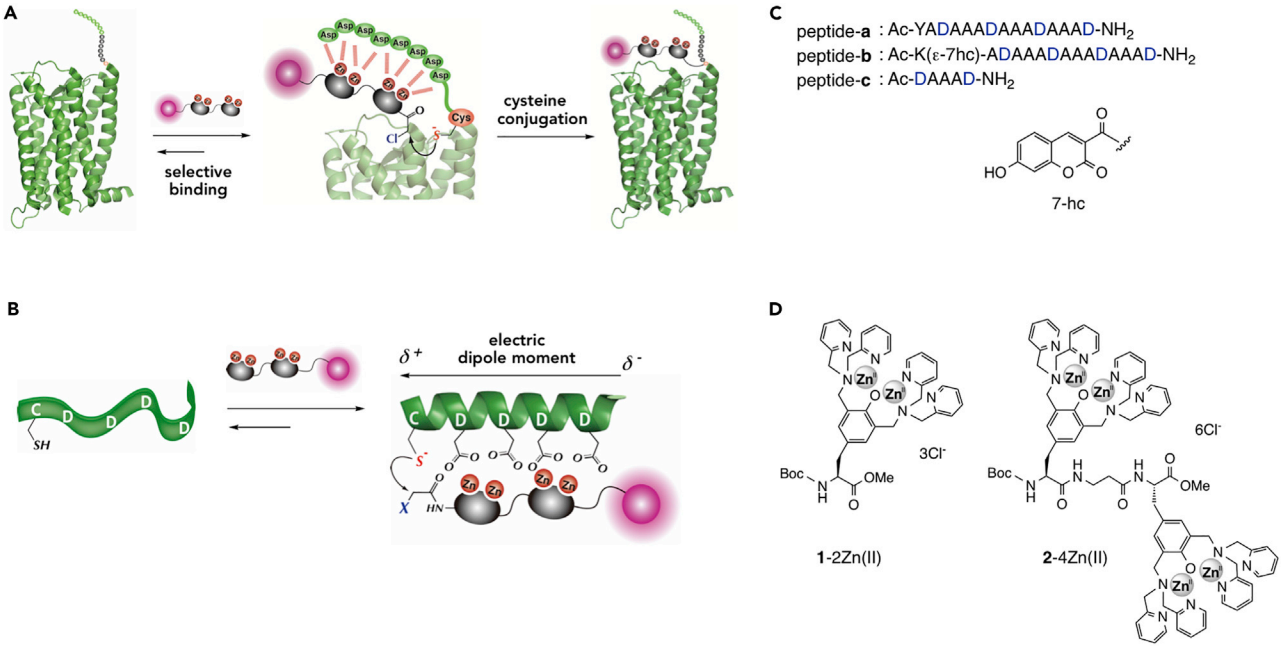

Figure 1. Specific Labeling of Protein Utilizing Complementary Recognition Pair of Peptide Tag and Reactive Zinc Complex

(A) Schematic illustration of covalent labeling of tag-fused protein with zinc complex probe.

(B) Binding-induced cysteine conjugation of α-helical peptide tag with zinc complex probe developed in the current study.

(C) Sequences of the peptide tags.

(D) Structures of the Zn(II)-DpaTyr probes.

approach, various enzyme-mediated labeling methods for tag-fused proteins (SNAP-tag, Halo-tag, and lipoic acid ligase) have also been developed (Walper et al., 2017). Compared with these enzymatic approaches, the chemical labeling methods using the tag-probe pair benefit from high tolerability of labeling conditions (including pH, solvent composition, chemical fixation), flexibility in probe design independent from substrate specificity of enzymes, and small molecular size of the tag and the probe, which allows location of the labeled probe at close position to POI. All these properties would increase utility of the chemical labeling method in high-resolution protein analysis by EM, which often needs to handle chemically fixed cell and tissue.

We have previously reported the selective covalent labeling of protein using a complementary recognition pair of a peptide tag and a reactive zinc complex (Figure 1A) (Nonaka et al., 2010). In this tag-probe pair, the interaction between the aspartate-rich peptide tag (D4-tag; CAAAAAADDDDGDDDD) and the tetranuclear zinc complex (Zn(II)-DpaTyr) induces their cysteine conjugation. However, the overly reactive α-chloroacetamide group of the zinc complex often induced non-specific labeling, hampering its wide use in fluorescence analysis of proteins. This problem prompted us to develop a new tag-probe pair, which has an improved labeling selectivity while retaining a high reactivity. In this manuscript, we report the development of a new peptide tag-probe pair for specific protein labeling and its application to EM detection of membrane proteins at single-molecular level. The high labeling selectivity of this chemical labeling overcame the problem of the non-specific labeling, enabling EM detection of the labeled G protein-coupled receptor (GPCR) in cell membrane freeze-fracture replicas and ultrathin sections. The efficiency and resolution obtained by the chemical labeling was significantly higher than those obtained by the immunogold labeling. The chemical labeling method also revealed high-density clusters of molecules closer than a few nanometers to each other, demonstrating its utility in single protein detection by EM.

RESULTS AND DISCUSSIONS

Design of α-Helical Peptide Tag

The selective chemical labeling of proteins would be achieved by utilizing a pair of highly reactive peptide tag and probe with a tuned weak reactivity. On the basis of this strategy, we initially developed a highly

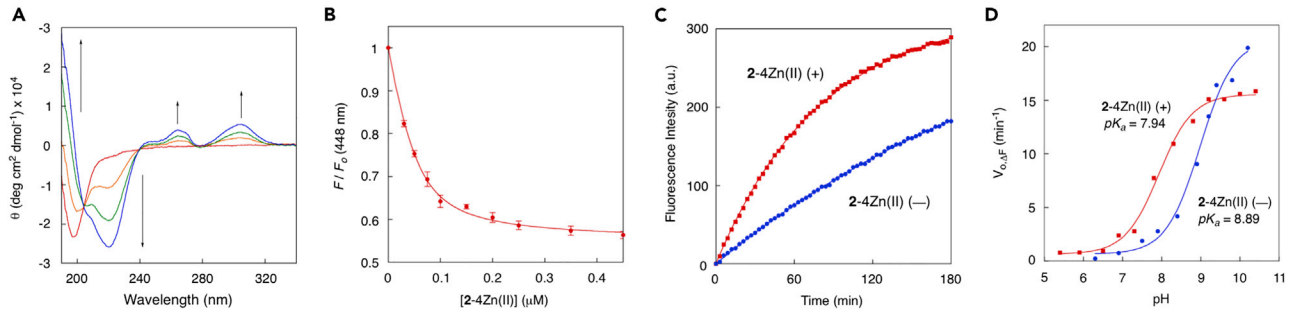

Figure 2. Binding and Reactivity Profiles of Aspartate-Rich Peptide Tags

(A) CD spectral change of peptide-**a** upon the addition of **1**-2Zn(II). Conditions: [peptide-**a**] = 50 μM, [**1**-2Zn(II)] = 0, 25, 50, and 100 μM, 10 mM borate buffer, pH 8.0, 25°C.

(B) Fluorescence titration profile of peptide-**b** (λ_{em} = 448 nm) upon the addition of **2**-4Zn(II). Conditions: [peptide-**b**] = 0.05 μM, 50 mM HEPES buffer, 100 mM NaCl, pH 7.2, 25°C. Each plot represents the average value ±standard error of triplicate experiments.

(C) Time-trace plot of the reaction of peptide-**d** with fluorogenic mCBI in the presence or absence of **2**-4Zn(II). Conditions: [peptide-**d**] = 4 μM, [mCBI] = 120 μM, [**2**-4Zn(II)] = 14 μM, 50 mM HEPES, 100 mM NaCl, pH 7.2, 37°C.

(D) Plot of pH-dependent reaction rate ($V_{o,\Delta F}$) of peptide-**d** with mCBI in the presence or absence of **2**-4Zn(II). Data were analyzed using Henderson-Hasselbach equation.

reactive peptide tag with a low pK_a value of the cysteine residue. The pK_a value of a cysteine thiol is typically around 8.5, which indicates that the cysteine residue mainly exists as a weakly reactive sulfhydryl form (R-SH) under neutral physiological conditions (pH = *ca.* 7.4). It is known that an N-terminal cysteine residue of an α-helix possesses a low pK_a value because of the strong electric dipole moment along the helical axis (Figure 1B) (Kortemme and Creighton, 1995). On this basis, we initially designed peptide-**a** with four aspartates at *i*, *i+4* position (Figure 1C). Conformational change of peptide-**a** upon interaction with the binuclear zinc complex **1**-2Zn(II) (Figure 1D) was analyzed by circular dichroism (CD) (Figure 2A). Peptide-**a** existed as a random coil in native state, as indicated by the CD spectrum (10 mM borate buffer, pH 8.0). However, upon the addition of **1**-2Zn(II), the characteristic signals of α-helix were observed at 190, 208, and 222 nm in the CD spectrum, with a concomitant appearance of the induced CD (*i*-CD) peaks at 264 and 303 nm in the absorption region of **1**-2Zn(II). A similar CD signal was also induced by the dimer-type zinc complex **2**-4Zn(II) (Figure S1). The binding affinity of **2**-4Zn(II) to peptide-**a** was estimated to be 1.37×10^7 $M^{-1}$by fluorescence titration of peptide-**b**, bearing a fluorescent 7-hydroxycoumarin (7-hc) (Figure 2B). This binding affinity was approximately 2000-fold higher than that of the binuclear **1**-2Zn(II) and the short peptide-**c** ($K_a = 7.04 \times 10^3$ M^{-1}), as determined by isothermal titration calorimetry measurement (Figure S2). These data suggested that multiple coordination interactions cooperatively work in the binding complex of **2**-4Zn(II) and peptide-**a** to afford the strong binding affinity.

Design of Peptide Tag with a Highly Reactive Cysteine

We next evaluated the pK_a value of the cysteine residue in the aspartate-rich peptides by using fluorogenic monochlorobimane (mCBI). As shown in Figure 2C, the initial reaction rate of the peptide-**d** with mCBI ($V_{o,\Delta F}$, min^{-1}) increased with rising pH (Figure 2D), and the analysis of the pH-dependent plot using Henderson-Hasselbalch equation determined its cysteine pK_a value to be 8.89 (Table 1) (Bulaj et al., 1998). Interestingly, this pK_a value decreased to 7.94 in the presence of **2**-4Zn(II), suggesting that the α-helical conformation induced by **2**-4Zn(II) stabilized the thiolate anion due to the helix dipole moment.

We then modified the sequence of peptide-**d** to lower the pK_a of the cysteine thiol. It is known that the family of glutaredoxin proteins share a common -Cys-Pro-Xaa-Cys- motif in the active site and that the cysteine thiol positioned at the N terminus of an α-helix has an extremely low pK_a value (*ca.* 3.8) (Jao et al., 2006; Floppe and Nilsson, 2007). On this basis, we designed peptide-**e** (Table 1) with an N-terminal -Cys-Pro-Tyr-Ala- sequence mimicking yeast glutaredoxin. The pK_a of the cysteine thiol of peptide-**e** in the absence of **2**-4Zn(II) was determined to be 8.48, which was lower by approximately 0.4 pH unit than that of peptide-**d** (pK_a = 8.89). Another strategy of lowering the pK_a value of cysteine thiol was the introduction of a positively charged amino acid, which can electrostatically stabilize an adjacent cysteine residue (Lutolf et al., 2001). We thus designed peptide-**g** and peptide-**h**, which possess two Lys or Arg residues at the N termini, respectively. The pK_a values of these peptides (pK_a = 8.04 and 8.02, respectively) were apparently lower than that of peptide-**e** (pK_a = 8.48), indicative of electrostatic stabilization of the thiolate anion by the

	2-4Zn(II) (−)		2-4Zn(II) (+)	
	pK_a	k ($\times 10^{-2}$, s^{-1})[a]	pK_a	k ($\times 10^{-2}$, s^{-1})[a]
peptide-**d**: Ac-YG**C**AAADAAADAAADAA AD-NH_2	8.89	0.66	7.94	1.51
peptide-**e**: Ac-GG**C**PYADAAADAAADAA AD-NH_2	8.48	2.00	7.46	5.11
peptide-**f**: Ac-YG**C**PAADAAADAAADAA AD-NH_2	8.93	0.37	7.80	1.24
peptide-**g**: Ac-KK**C**PYSDAAADAAADAA AD-NH_2	8.04	2.51	7.13	7.60
peptide-**h**: Ac-RR**C**PYSDAAADAAADAA AD-NH_2	8.02	2.92	7.18	6.72
peptide-**i**: Ac-YG**C**AAAAAADDDDGDD DD-NH_2	8.96	1.17	8.22	1.78

Table 1. Summary of the pK_a Values of the Cysteine Residue in the Peptides, and the First-Order Reaction Rate Constants (k, s^{-1}) with mCBI in the Presence or Absence of 2-4Zn(II)

[a]Measurement conditions: 50 mM HEPES, 100 mM NaCl, pH 7.2, 37°C.

positively charged amino acid residues. Most interestingly, the pK_a values of all peptides largely decreased by approximately 1 pH unit in the presence of **2**-4Zn(II). The lowest pK_a value (pK_a = 7.13) was observed in the binding complex of peptide-**g** with **2**-4Zn(II). Conversely, the previously developed peptide-**i** (D4-tag) (Nonaka et al., 2010) showed the highest pK_a value (pK_a = 8.22) among the peptides.

The first-order reaction rate constant (k, s^{-1}) of the peptides with mCBI under neutral aqueous solution (50 mM HEPES, 100 mM NaCl, pH 7.2, 37°C) is summarized in Table 1. Notably, the reaction rate order correlated well with that of the pK_a value of the cysteine thiol. That is, a peptide with a low pK_a exhibited high reactivity, suggesting that the thiolate anion served as the main reactive species in the nucleophilic reaction with mCBI. Furthermore, **2**-4Zn(II) accelerated the reaction of all α-helical peptides (peptides-**d**–**h**) with mCBI, consistent with their low pK_a values in the binding complex. The most reactive peptide was peptide-**g**: its reaction rate in the presence of **2**-4Zn(II) (k = 7.60 × 10^{-2} s^{-1}) was over ten times higher than that of the initially designed peptide-**d** in the absence of **2**-4Zn(II) (k = 0.66 × 10^{-2} s^{-1}). These observations demonstrated the validity of our strategy to gain a highly reactive peptide tag by lowering the pK_a value of the cysteine.

Tuning of Probe Reactivity for Enhanced Labeling Selectivity

To reduce the non-specific labeling activity of the Zn(II) complex, we next tuned its reactivity. Michael acceptor is an important class of reactive group for cysteine thiol and has been widely used for protein modification with synthetic probes and covalent drugs (Singh et al., 2010). Considering the broad tunability of its reactivity (Flanagan et al., 2014), we prepared the monomer-type zinc complexes **3**-2Zn(II) to **5**-2Zn(II) bearing a different Michael acceptor group (Figure S3) and evaluated their reactivity with peptide-**g** by using mCBI. The kinetic analysis revealed that the reactivity of **5**-2Zn(II) ($t_{1/2}$ = 3.98 h) bearing a γ-dimethylaminocrotonate (DMAC) (Wissner et al., 2003) as Michael acceptor group was substantially lower than that of α-chloroacetamide **6**-2Zn(II) ($t_{1/2}$ = 0.20 h). These data suggested the potential utility of DMAC as a reactive group of the labeling probe with a moderate reactivity. The other Michael acceptor-type probes 3-2Zn(II) and 4-2Zn(II), which bears a cinnamide and crotonamide, respectively, showed the low reactivity with peptide-**g** ($t_{1/2}$ > 24 h).

We next evaluated the reactivity of dimer-type zinc complexes **7**-4Zn(II) to **9**-4Zn(II) bearing a DMAC group (Table 2). Their reactivity was evaluated with peptide-**g** to peptide-**i**, which possessed the different number of alanine residue(s) for optimization of spatial orientation between the cysteine residue and the bound Zn(II) complex. Interestingly, the reactivity was greatly affected by the structure of the Zn(II) complex: the reaction rate of **9**-4Zn(II), possessing a rigid L-proline linker, with peptide-**g** ($t_{1/2}$ = 0.74 h) was higher than that of **7**-4Zn(II) ($t_{1/2}$ = 3.3 h). In contrast, **8**-4Zn(II) possessing an ethylene glycol linker exhibited a

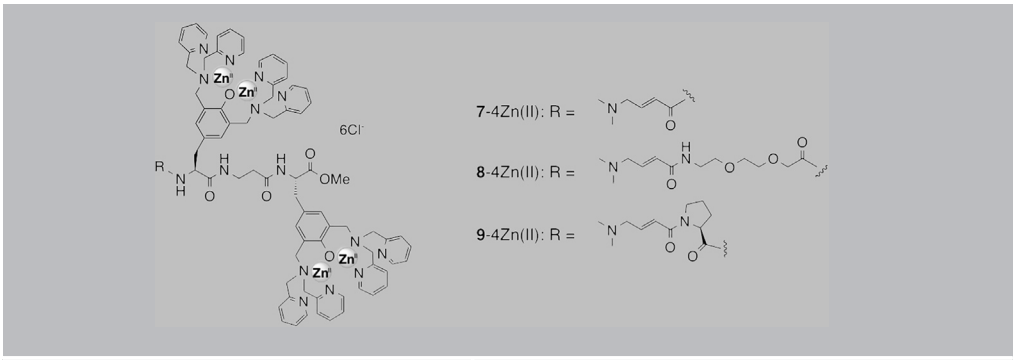

	$t_{1/2}$ (h)		
	7-4Zn(II)	8-4Zn(II)	9-4Zn(II)
peptide-**g**: Ac-KK**C**PYSDAAADAAADA AAD-NH_2	3.30	13.9	0.74
peptide-**j**: Ac-KK**C**PYSADAAADAAADA AAD-NH_2	2.69	16.0	0.24
peptide-**k**: Ac-KK**C**PYSAADAAADAAADA AAD-NH_2	1.96	9.84	0.22
peptide-**i**: Ac-YG**C**AAAAAADDDDGD DDD-NH_2	6.78	–[a]	2.84

Table 2. Summary of the Reaction Half-Time ($t_{1/2}$, h) of the Zinc Complexes with the Peptides
Measurement conditions: 50 mM HEPES, 100 mM NaCl, pH 7.2, 37°C.
[a]Not determined.

much lower reactivity ($t_{1/2}$ = 13.9 h). The reactivity was also influenced by the number of inserted alanine(s) in the peptide tag: peptide-**k**, which possessed two additional alanine residues, showed a higher reactivity ($t_{1/2}$ = 0.22 h) for **9**-4Zn(II) compared with peptide-**g** ($t_{1/2}$ = 0.74 h). Consequently, **9**-4Zn(II) and peptide-**k** were identified as the optimized tag-probe pair with the highest reactivity. We confirmed that the pK_a values of peptides with inserted alanine(s) (peptide-**j** and -**k**) in a binding complex with **2**-4Zn(II) were 7.08 and 7.14, respectively, which were comparable with that of peptide-**g** (pK_a = 7.13) (Figure S4). Overall, the reactivity of the optimized tag-probe pair (i.e., **9**-4Zn(II) and peptide-**k**, $t_{1/2}$ = 0.22 h) was approximately 30-fold higher than that of the previously developed D4-tag peptide-**i** with the structurally unoptimized **7**-4Zn(II) ($t_{1/2}$ = 6.78 h, Table 2).

Fluorescence Labeling of HelixD2-Tag-Fused Protein

The optimized tag-probe pair was used for fluorescence labeling of tag-fused proteins. We first employed maltose-binding protein (MBP) tagged with the 21-amino acid peptide-**k**, named helixD2-tag (KKCPYSAA DAAADAAADAAAD). The labeling reaction of helixD2-MBP was conducted with the fluorescent zinc complex **10**-4Zn(II) bearing an Oregon green 488 under aqueous buffer conditions (50 mM HEPES, 100 mM NaCl, pH 7.2) (Figure 3A). In-gel fluorescent analysis revealed that the labeling reaction proceeded in a time-dependent manner (Figures 3B and 3C). The half reaction time ($t_{1/2}$) was determined to be 0.28 h by pseudo-first-order kinetic analysis, which was comparable with that of the reaction between peptide-**k** and **9**-4Zn(II) ($t_{1/2}$ = 0.22 h, Table 2). The second-order reaction rate constant of the labeling reaction of helixD2-MBP with **9**-4Zn(II) was also determined to be 9.4 × 10^2 M^{-1} s^{-1} by the detailed kinetic analysis (Figure S5). A control labeling reaction was conducted using MBP tagged with the cysteine-containing histidine-rich peptide (CH6 tag; CHHHHHH). As shown in Figure 3B, no labeling adduct was detectable with CH6-MBP, consistent with the weak binding affinity of the zinc complex and hexahistidine peptide (K_a < 10^3 M^{-1}) (Uchinomiya et al., 2014).

We next applied the tag-probe pair to the covalent labeling of GPCR protein on the cell surface. In the experiment, bradykinin receptor type2 (B2R) was tagged with a helixD2-tag (located at the extracellular

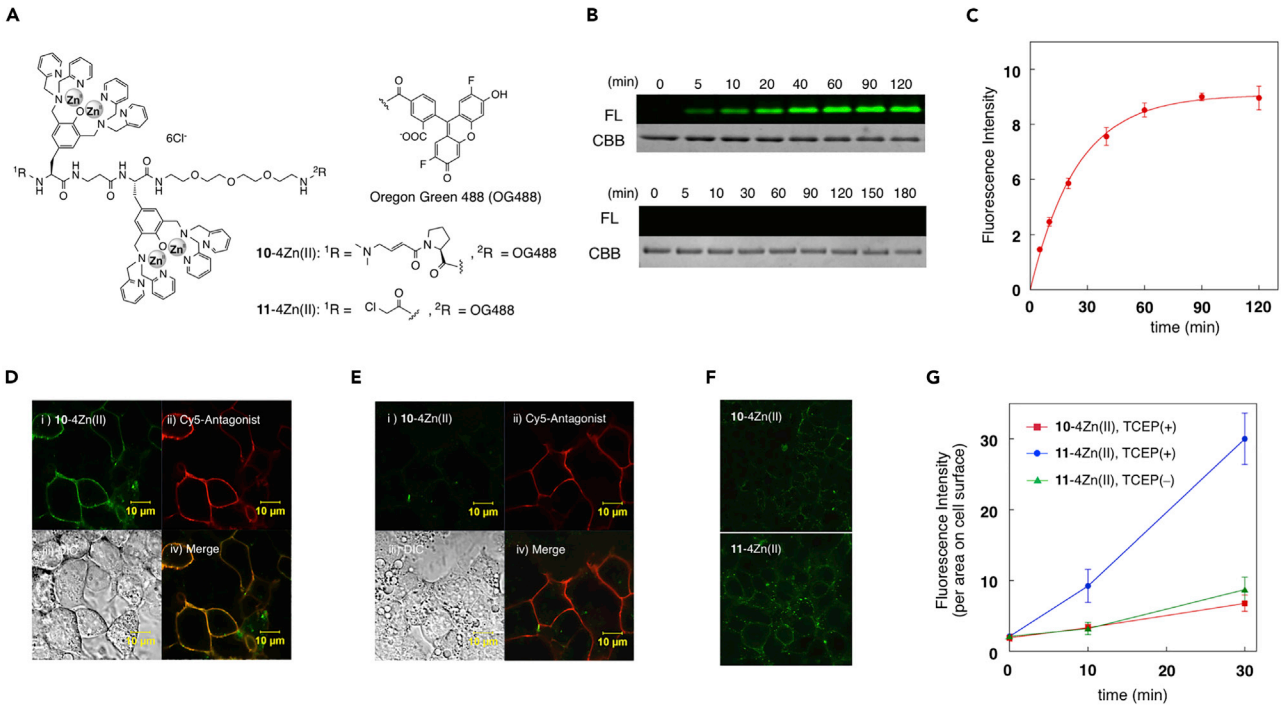

Figure 3. Fluorescence Labeling of helixD2-Tag-Fused Protein

(A) Structures of the fluorescent Zn(II)-DpaTyr probes.

(B) In-gel fluorescence (FL) and Coomassie Brilliant Blue (CBB) analysis of covalent labeling of MBP tagged with a helixD2-tag (upper panel) or CH6 tag (lower panel) by **10**-4Zn(II). Labeling conditions: [tag-MBP] = 1 μM, [**10**-4Zn(II)] = 10 μM, 50 mM HEPES, 100 mM NaCl, 20 mM TCEP, pH 7.2, 37°C.

(C) Time-trace plot of the fluorescence band intensity of the MBP labeled with **10**-4Zn(II) (mean ± SD of triplicate experiment).

(D and E) Fluorescence imaging of HEK293 cells expressing B2R fused with helixD2-tag (D) or CH6 tag (E) upon labeling with **10**-4Zn(II). Labeling conditions: [**10**-4Zn(II)] = 4 μM, HEPES-buffered saline, pH 7.4, 37°C, 30 min.

(F and G) (F) Fluorescence images of non-specific labeling on surface of HEK293 cells without expression of the tag-fused B2R. Labeling conditions: [**10**-4Zn(II) or **11**-4Zn(II)] = 4 μM, HEPES-buffered saline, 20 μM TCEP, pH 7.4, 37°C, 30 min (G) Time-trace plot of the fluorescence intensity on the surface of HEK293 cells without expression of the tag-fused B2R (n = 10, mean ± SD).

N-terminal region of B2R) and transiently expressed in HEK293 cells. When the cells were pre-treated with tris(2-carboxyethyl)phosphine (TCEP) to activate the cysteine residue of the tag, and then incubated with 4 μM of **10**-4Zn(II) for 30 min at 37°C, the bright fluorescence signal was observed on the cell surface (Figure 3D). The obtained fluorescence image overlapped well with that of the fluorescent B2R antagonist peptide, indicative of selective covalent labeling of the tag-fused B2R by **10**-4Zn(II). The fluorescence of **10**-4Zn(II) was not observed on the cell surface when the labeling reaction was conducted in the presence of 1 mM inorganic pyrophosphate (PPi), a strong binder to the zinc complex (Figure S6). Similarly, the labeling of HEK293 cells expressing B2R tagged with CH6 did not show any fluorescence on the cell surface (Figure 3E). These data suggest that the selective binding between the helixD2-tag and **10**-4Zn(II) is essential for the efficient covalent labeling of B2R.

To evaluate the non-specific labeling activity of the probes on the cell surface, HEK293 cells that did not express B2R were treated with **10**-4Zn(II) or α-chloroacetamide probe **11**-4Zn(II) (4 μM, 37°C), and the fluorescence of the cell surface was quantified by confocal microscopy with a high laser power after formaldehyde fixation (Figures 3F and 3G). The result revealed that the fluorescence of **10**-4Zn(II) associated with non-specific reaction was apparently weaker than that of the highly reactive **11**-4Zn(II). Furthermore, **11**-4Zn(II) induced a noticeable time-dependent increase of the fluorescence signal on the cell surface. These data clearly indicated that non-specific labeling activity of **10**-4Zn(II) was significantly lower than that of **11**-4Zn(II). The fluorescence of **11**-4Zn(II) substantially decreased without the reductive treatment with TCEP, implying that cysteine residue of membrane proteins was the major non-specific labeling site. The weak non-specific reactivity of **10**-4Zn(II) was also confirmed by the labeling experiment of the helixD2-MBP under E. *coli* lysate conditions (Figure S7). In-gel fluorescence analysis of the lysate sample

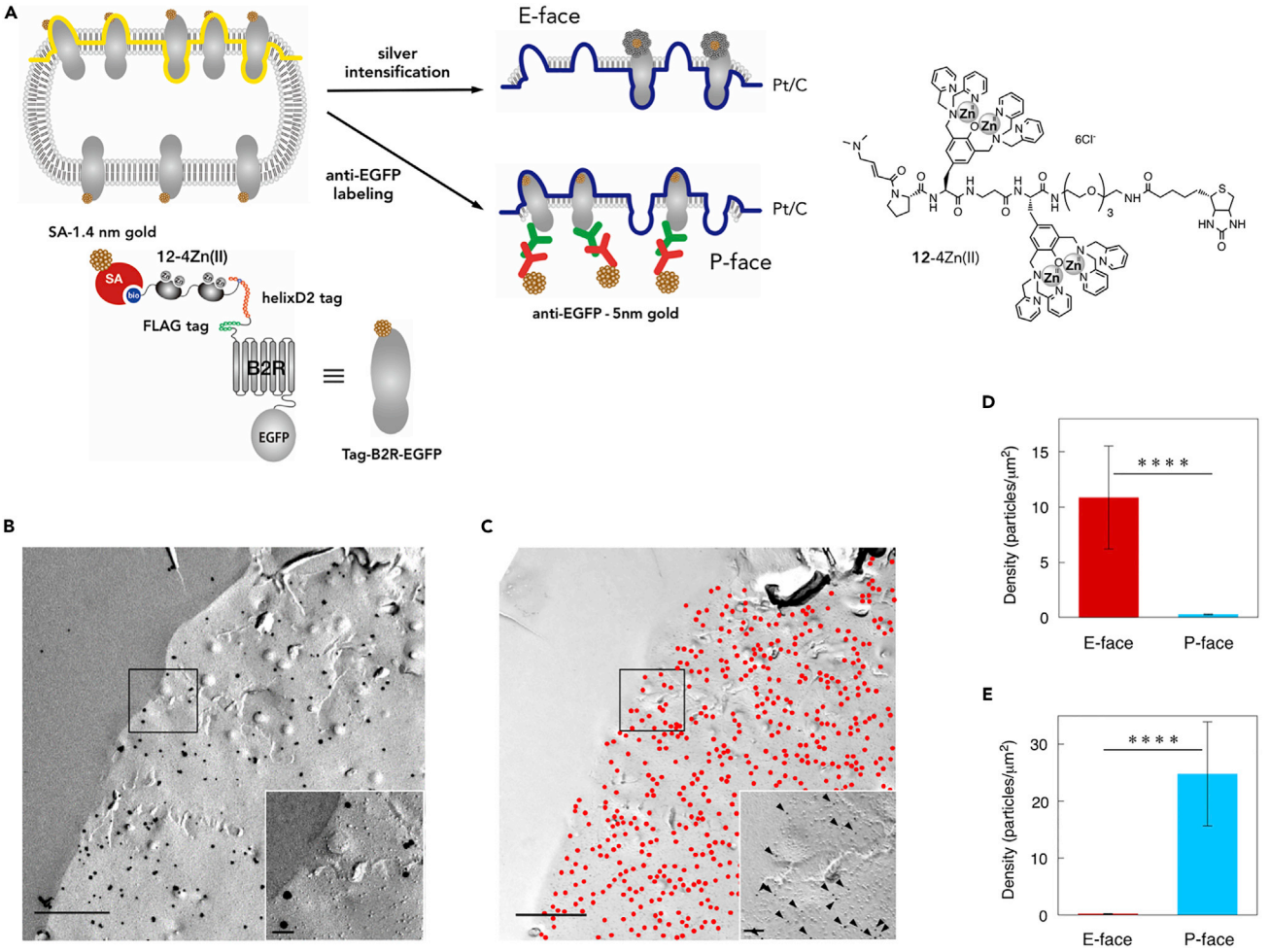

Figure 4. EM Detection of helixD2-Tag-Fused B2R Protein on Freeze-Fracture Replicas

(A) Schematic illustration of labeling states of a complementary replica pair.

(B and C) EM images of the complementary replicas showing E-face (B) and P-face (C) from the same membrane. Scale bars, 1 μm. (Insets) Magnified images of the area framed in the main pictures. Arrowheads indicate 5-nm gold particles. Scale bars, 100 nm.

(D) Comparison of the labeling density of **12**-4Zn(II) on the E- and P-face images, respectively (****$p < 0.001$, Mann-Whitney U test; E-face, n = 11; P-face, n = 9, mean ± SE).

(E) Comparison of the labeling density of anti-GFP antibody on the E- and P-face images, respectively (****$p < 0.001$, Mann-Whitney U test; E-face, n = 7; P-face, n = 15, mean ± SE).

revealed that the band intensities of proteins non-specifically labeled by **10**-4Zn(II) were significantly lower than those labelled by **11**-4Zn(II).

EM Detection of Tag-Fused Protein Using Biotin and Nanogold-Conjugated Probes in Freeze-Fracture Replica

We applied chemical labeling to EM detection in combination with sodium dodecyl sulfate (SDS)-digested freeze-fracture replica labeling (SDS-FRL) technique (Fujimoto, 1995). This technique is widely used to detect the two-dimensional distribution of membrane proteins on protoplasmic (P-) and exoplasmic (E−) leaflet of lipid bilayer in freeze-fracture replicas (Meier and Beckmann, 2018). In the current study, we first used the biotin probe **12**-4Zn(II) to detect helixD2-B2R-EGFP, which harbored an extracellular N-terminal helixD2-tag and an intracellular C-terminal enhanced green fluorescent protein (EGFP) (Figure 4A). The labeling specificity of **12**-4Zn(II) toward helixD2-B2R-EGFP was confirmed by fluorescence imaging using Alexa Fluoro 633-conjugated streptavidin (SA) (Figure S8). For EM detection, helixD2-B2R-EGFP, expressed on the surface of live HEK293 cells, was labeled with **12**-4Zn(II) followed by secondary labeling with SA-conjugated 1.4-nm gold particle. After fixation with paraformaldehyde, a complementary

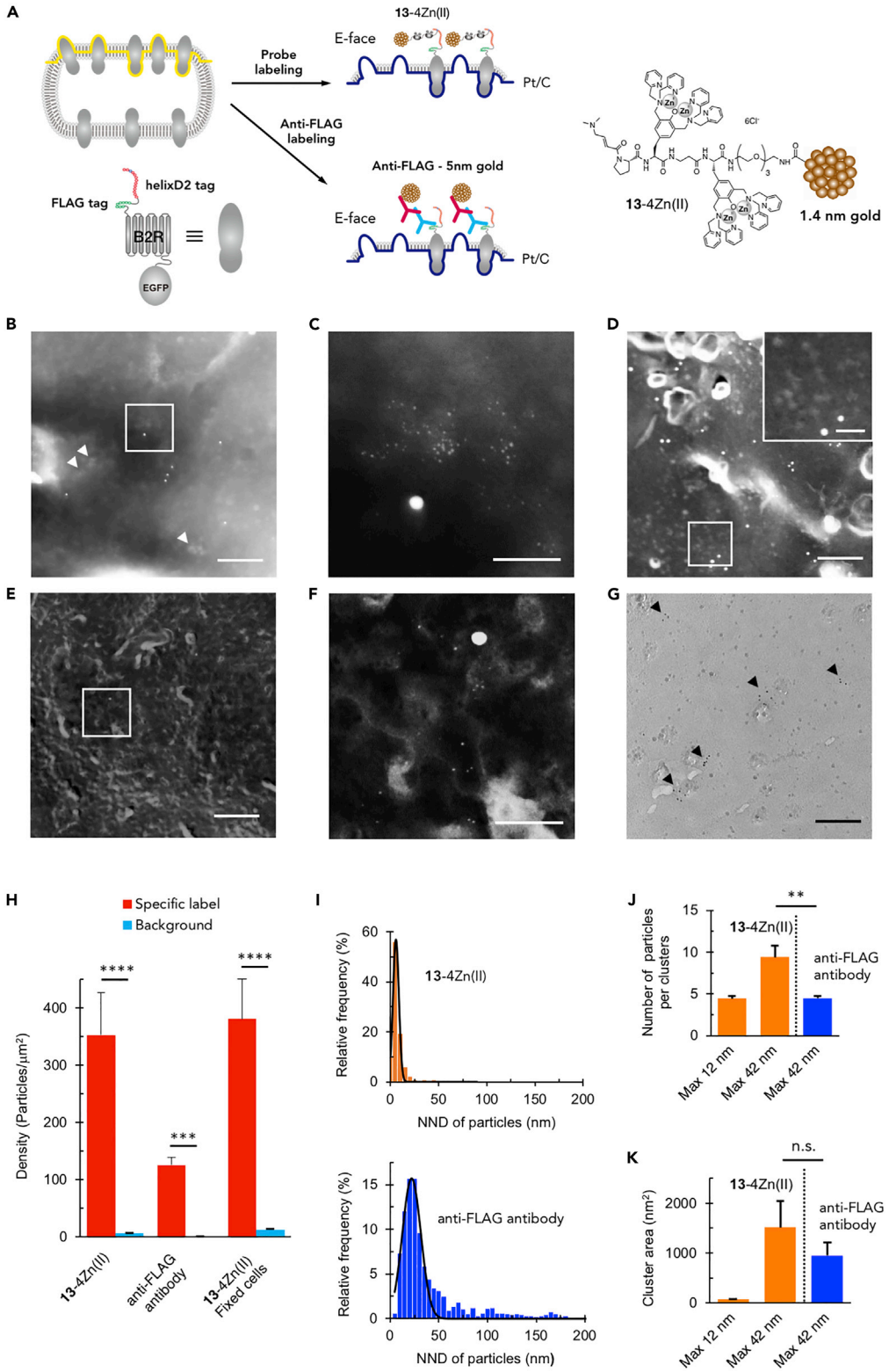

Figure 5. EM Detection of helixD2-Tag-Fused B2R Protein on HEK Cells Using the Probe Conjugated with a 1.4-nm Gold Particle

(A) Schematic illustration of labeling states of replicas.

Figure 5. *Continued*

(B–D) Dark-field scanning transmission electron microscopy images of E-face replicas made from transfected (B and C) or non-transfected (D) HEK cells labeled with **13**-4Zn(II) before aldehyde fixation. (C) and the inset on (D) are magnified images of the area framed in (B) and (D), respectively. White arrowheads indicate B2R clusters labeled with **13**-4Zn(II). Scale bar: 200 nm in (B) and the main picture of (D) and 50 nm in (C) and the inset on (D).

(E and F) Dark-field images of replicas made from transfected HEK cells labeled with **13**-4Zn(II) after aldehyde fixation. (F) A magnified image of the area framed in (E). Scale bar: 200 nm in (E) and 50 nm in (F).

(G) Bright-field TEM image of E-face replica labeled with anti-FLAG antibody combined with 5-nm gold-particle-conjugated secondary antibody. Black arrowheads indicate B2R clusters labeled with 5-nm gold particles. Scale bar, 200 nm.

(H) Comparison of the specific and background labeling density with **13**-4Zn(II) and anti-FLAG antibody. "**13**-4Zn(II)" and "**13**-4Zn(II), fixed cells" indicate results from HEK cells labeled before and after aldehyde fixation, respectively (**13**-4Zn(II), ****$p < 0.001$, Mann-Whitney U test; specific labeling, n = 9 cells; background labeling, n = 13 cells; mean ± SE, anti-FLAG, ***$p < 0.005$, Mann-Whitney U test; specific labeling, n = 7 cells; background labeling, n = 7 cells; mean ± SE, **13**-4Zn(II), fixed cells, ****$p < 0.001$, Mann-Whitney U test; specific labeling, n = 11 cells; background labeling, n = 15 cells; mean ± SE).

(I) Distribution histograms of nearest neighbor distance (NND) of gold particles observed on replicas labeled with **13**-Zn(II) (upper, n = 1748 particles) and anti-FLAG antibody (bottom, n = 998 particles). Fitted lines show Gaussian distribution fitting for the peaks.

(J) Comparison of the number of particles per B2R cluster labeled with **13**-4Zn(II) and anti-FLAG antibody. "Max 12 nm" and "Max 42 nm" mean the maximum NND of gold particles used for the definition of clusters labeled with **13**-4Zn(II) and anti-FLAG antibody (**13**-4Zn(II) Max 12 nm; n = 10 cells, **13**-4Zn(II) Max 42 nm, n = 10 cells; anti-FLAG Max 42 nm, n = 7 cells, mean ± SE, **$p < 0.01$, Mann-Whitney U test).

(K) Comparison of the B2R cluster area evaluated by chemical labeling with **13**-4Zn(II) and immunolabeling with anti-FLAG antibody (**13**-4Zn(II) Max 12 nm; n = 10 cells; **13**-4Zn(II) Max 42 nm, n = 10 cells; anti-FLAG 42 nm, n = 7 cells; mean ± SE, n.s. $p > 0.05$, Mann-Whitney U test).

pair of P- and E-face freeze-fracture replica was prepared using the double replica method (Figure 4A). One replica of the pair underwent silver enhancement to increase the visibility of 1.4-nm gold particles labeled by the chemical labeling on the E-face. In another replica of the pair, EGFP was immunolabeled with 5-nm gold particles to detect helixD2-B2R-EGFP on the P-face. EM analysis revealed selective labeling of the helixD2-tag by the probe on the E-face (Figures 4B and 4D) and vice versa, selective labeling of EGFP on the corresponding P-face (Figures 4C and 4E). These observations are consistent with the extracellular location of the helixD2-tag and the intracellular location of EGFP.

Although the density of gold particles looked higher for EGFP than helixD2-tag, it is necessary to visualize each of them on the E-face to compare the labeling efficiency, because the allocation of helixD2-B2R-EGFP to the P-face and E-face can be different. In addition, binding of the biotin probe **12**-4Zn(II) and SA-conjugated particle can be disrupted by SDS treatment at 60°C reducing the labeling efficiency. Thus, we next used **13**-4Zn(II), which possesses a directly conjugated 1.4-nm nanogold particle to label helixD2-B2R-EGFP, and anti-FLAG antibody to label FLAG tag, which was inserted just next to the helixD2 tag in the extracellular domain of B2R (Figure 5A). Probe **13**-4Zn(II) was obtained by conjugation reaction of the amine probe **14**-4Zn(II) with mono-sulfo-N-hydroxy-succinimide nanogold particles in HEPES buffer (pH 8.0), which was followed by dialysis to remove the excess of **14**-4Zn(II). The labeling reaction of **13**-4Zn(II) was conducted for an extended time (2 h, 37°C) to fully label helixD2-B2R-EGFP expressed on HEK293 cells. To facilitate searching for E-face labeled with 1.4-nm gold particles by 200kV scanning transmission electron microscope (dark field mode), GluA2 subunit of α-amino-3-hydroxy-5-methyl-4-isoxazole-propionic acid-type glutamate receptor was co-expressed with helixD2-B2R-EGFP in HEK cells and labeled with 10-nm gold particles by an antibody for an extracellular epitope of GluA2 combined with anti-rabbit 10-nm gold particle-conjugated secondary antibody (Figure S9). On GluA2-labeled E-face, we found numerous 1.4-nm gold particles, often making high-density clusters of particles (Figures 5B and 5C). The specificity of the labeling was confirmed using HEK cells transfected with GluA2 but not with helixD2-B2R-EGFP (Figure 5D). The density of background labeling (5.9 particles/μm^2) was 1.7% of the specific labeling (353 particles/μm^2) (Figure 5H). In the immunogold labeling, the specific labeling by anti-FLAG tag antibody was observed on the E-face with 5-nm particles (125 particles/μm^2, n = 7 cells, Figure 5H), also showing clusters of particles (arrowheads in Figure 5G). The average density of B2R labeled with **13**-4Zn(II) was 2.8 times higher than that with anti-FLAG antibody (Figure 5H, $p < 0.05$).

To compare the clusters of particles obtained with the chemical labeling and anti-FLAG immunolabeling, we first examined nearest neighbor distance (NND) distributions of particles and found sharper peak at

smaller NND for the chemical labeling (8.6 ± 10.8 nm, mean ± SD, n = 1748 particles) than immunolabeling (47.4 ± 56.1 nm, mean ± SD, n = 998 particles, $p < 0.001$, Mann-Whitney U test) (Figure 5I). For defining the clusters, we fitted these peaks with Gaussian distribution and used mean + 2 SD as maximum distances allowed and three particles per cluster as a minimum number of particles per cluster (Miki et al., 2017). In case we use definition of clusters with different mean + 2 SD values for chemical labeling (12 nm) and immunolabeling (42 nm), the numbers of particles per cluster were similar (Figure 5J) but the cluster area was much smaller for chemical labeling (70 nm^2) than for immunolabeling (950 nm^2, Figure 5K), indicating that the clusters detected by chemical labeling represent subclusters consisting single clusters detected by immunolabeling. In case we use the same definition of clusters obtained by immunolabeling for both (42 nm as a maximum distance allowed), the cluster areas became similar and the number of particles per cluster was twice higher for chemical labeling than for immunolabeling (9.4 ± 1.4 particles, n = 10 cells for chemical labeling, 4.5 ± 0.3 particles, n = 7 cells for immunolabeling, mean ± SE, $p < 0.01$, Mann-Whitney U test, Figures 5J and 5K). Altogether, these results indicate higher labeling efficiency and detectability of high-density nanoclusters of proteins for chemical labeling with the probe directly conjugated with 1.4-nm nanogold particle than the immunolabeling with 5-nm gold-particle-conjugated secondary antibody.

In typical SDS-FRL experiment, biological samples, such as sliced tissue, are initially fixed with aldehyde to maintain protein location by physical stabilization (Masugi-Tokita and Shigemoto, 2007). Therefore, we next applied the chemical labeling to the fixed cell samples. HEK293 cells expressing helixD2-B2R-EGFP were first fixed with 2% paraformaldehyde and then labeled with **13**-4Zn(II). We found specific labeling for helixD2-B2R-EGFP with the fixed cells comparable with that obtained with living cells (Figures 5E, 5F, and 5H). This was indicative of the compatibility of the developed chemical labeling with aldehyde fixation. Since the majority of the existing enzyme-mediated and ligand-directed protein labeling methods (Walper et al., 2017; Matsuo and Hamachi, 2017) are difficult to apply to denatured proteins by fixation, these results demonstrated the high utility of the chemical labeling method for SDS-FRL using fixed biological samples.

EM Detection of Tag-Fused Protein Using Nanogold-Conjugated Probes in Ultrathin Section

To further confirm higher resolution of the chemical labeling using **13**-4Zn(II), we performed EM analysis of ultrathin sections of resin-embedded HEK293 cells. We compared the distances from the silver-intensified 1.4-nm gold particles to cell membrane between the samples labeled by **13**-4Zn(II) and those labeled by anti-FLAG antibody combined with 1.4-nm gold-particle-conjugated secondary antibody (Figures 6A and 6C). The background density of particles examined in non-transfected cells was 0.8% and 0.6% of the specific labeling by **13**-4Zn(II) and anti-FLAG antibody, respectively. The silver-intensified gold particles appeared to be mostly attached to the cell membrane in the chemical labeling (Figure 6B), whereas those in the FLAG immunolabeling showed apparent gaps between the particles and the cell membrane (Figure 6D). Considering that silver intensification may occur in a non-isotropic/concentric manner around 1.4-nm gold particles, we used minimum time (3–6 min) for silver intensification and examined the correlation of the size of silver-intensified particles and the distance between the center of silver-intensified particles and the midpoint of lipid bilayer (Figure 6E). We found a significant positive correlation for both chemical labeling ($r_s = 0.24$, $p < 0.01$, n = 147 particles) and immunolabeling ($r_s = 0.26$, $p < 0.01$, n = 228 particles). By extrapolating linear fits, estimated distances of non-intensified 1.4-nm particles were calculated to be 5.4 nm and 9.9 nm for chemical labeling and immunolabeling, respectively. Since the half thickness of lipid bilayer was estimated to be 4 nm by EM analysis (Robertson, 1958), the distance of 1.4-nm gold particles from the cell surface was deduced to be 1.4 and 5.9 nm for the chemical labeling and immunolabeling, respectively (Figure 6E). Although direct comparison of the distances from these labels to the respective tags is not possible because the exact tag positions are unknown, the variance of the measured distances is significantly smaller for **13**-4Zn(II) than for anti-FLAG antibody ($F_{227, 146} = 2.0$, $p < 0.001$), indicating higher resolution of the chemical labeling method than the immunolabeling method (Figure 6F).

Conclusion

In summary, we have achieved EM detection of GPCR by chemical labeling using a reactive peptide tag-probe pair. Rational design of the highly reactive α-helical peptide tag and the fine-tuning of probe reactivity enabled the specific cysteine conjugation of the tag-fused B2R protein on cell surface. EM detection using the tag-probe pair was successfully applied to determine the localization of B2R receptor on cell surface with a high labeling specificity. Furthermore, the probe directly conjugated with a 1.4-nm gold particle

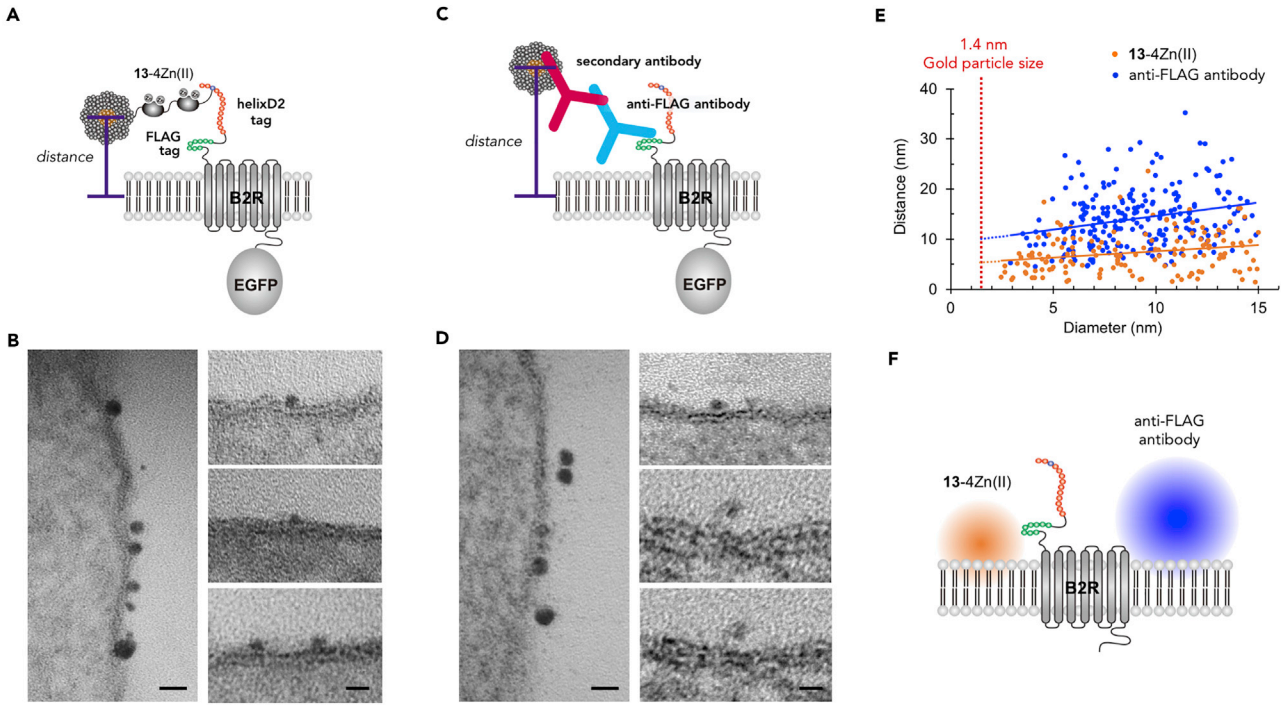

Figure 6. Comparison of Resolution between Chemical Labeling and Immunolabeling Methods

(A and C) Schematic illustration of labeling states of the tagged-B2R on HEK cells labeled with **13**-4Zn(II) (A) and anti-FLAG antibody combined with 1.4-nm gold-particle-conjugated secondary antibody (C).

(B and D) EM images of ultrathin sections prepared from HEK cells labeled with **13**-4Zn(II) (B) and anti-FLAG antibody (D), respectively. Gold particles were intensified by silver enhancement for 3–6 min. Distances between the particle center and the middle of the cell membrane were measured in sections tilted to obtain perpendicular views to the plasma membrane. Scale bars, 20 nm (left) and 10 nm (right).

(E) Correlation of the intensified particle size and distance between particle centers and the middle of the cell membrane (orange dots, **13**-4Zn(II); blue dots, anti-FLAG antibody). Significant positive correlation was detected for both (correlation coefficient = 0.24, $p < 0.01$, $n = 147$ for **13**-4Zn(II); correlation coefficient = 0.26, $p < 0.01$, $n = 228$ for anti-FLAG antibody, Pearson correlation analysis). The distances for non-intensified 1.4-nm particles were deduced from linear fits extrapolated (broken orange and blue lines) to 1.4 nm (red dotted line).

(F) Schematic illustration of positions of non-intensified 1.4-nm particles estimated by the two labeling methods in (E). The gradient circle indicates the deviation of the position.

enabled the detection of the membrane proteins with a few times higher labeling efficiency and significantly higher spatial resolution than that of the antibody-mediated labeling, revealing high-density nanoclusters of proteins. EM detection methods for in-cell proteins using genetically encoded peroxidases have been developed in recent years (Shu et al., 2011; Martell et al., 2012; Hainfeld and Powell, 2000). Despite their usefulness, these methods are hardly applicable to single-protein detection since they have been devised for EM contrast imaging based on OsO_4 staining in combination with oxidative diaminobenzidine (DAB) polymerization. To the best of our knowledge, the research presented herein is the first example of high-resolution single-protein detection by EM utilizing a chemical labeling. The use of our labeling method is currently limited to cell surface proteins. Nevertheless, this method can be widely used for EM analysis of membrane proteins on replicas in combination with SDS-FRL. We envision further application of the chemical labeling approach to reveal subunit composition of single-protein complexes on cell surface in combination with other tag-probe pairs (Uchinomiya et al., 2013).

Limitations of the Study

In our study, we demonstrate higher efficiency and resolution of the newly developed chemical labeling method compared with the common immunolabeling methods at the EM level using HEK cells expressing tagged B2R. Accurate evaluation of labeling resolution, however, requires understanding of the exact molecular structure of the tagged receptor. Since background and labeling conditions can be different between cell culture and various tissue environments, usefulness of the reported reactive peptide tag-probe pair needs further verification in more complex sample preparations.

METHODS

All methods can be found in the accompanying Transparent Methods supplemental file.

SUPPLEMENTAL INFORMATION

Supplemental Information can be found online at https://doi.org/10.1016/j.isci.2019.11.025.

ACKNOWLEDGMENTS

We thank David Kleindienst for technical support with the GPDQ software. This work was supported by the Grant-in-Aid for Scientific Research B (JSPS KAKENHI grant no. JP17H03090 to A.O.); the Scientific Research on Innovative Areas "Chemistry for Multimolecular Crowding Biosystems" (JSPS KAKENHI grant no. JP17H06349 to A.O.); and the European Union (European Research Council Advanced grant no. 694539 and Human Brain Project Ref. 720270 to R.S.). A.O. acknowledges the financial support of the Takeda Science Foundation.

AUTHOR CONTRIBUTIONS

A.O. and R.S. conceived of and directed the study. S.T., I.H., N.K., H.F., M.K., K.T., N.Z., and S.U. synthesized the compounds; designed and executed the chemical, biochemical, and cellular experiments; and analyzed the data. S.U. assisted in data analysis. M.I. developed the anti-GluA2 antibody. S.T., M.J., H.H., and R.S. performed the transmission EM imaging and the data analysis. A.O., R.S., S.T., and S.U. wrote the manuscript.

DECLARATION OF INTERESTS

The authors declare no competing interests.

Received: April 12, 2019
Revised: October 26, 2019
Accepted: November 12, 2019
Published: December 20, 2019

REFERENCES

Bulaj, G., Kirtemme, T., and Goldenberg, D.P. (1998). Ionization-reactivity relationship for cysteine thiol in polypeptides. Biochemistry *37*, 8965–8972.

Dean, K.M., and Palmer, A.E. (2014). Advances in fluorescence labeling strategies for dynamic cellular imaging. Nat. Chem. Biol. *10*, 512–523.

Faulk, P.W., and Taylor, M.G. (1971). An immunocolloid method for the electron microscope. Immunochem *8*, 1081–1083.

Fijita, A., Cheng, J., Hirakawa, M., Furukawa, K., Kusunoki, S., and Fujimoto, T. (2007). Ganglioside GM1 and GM3 in the living cell membrane from clusters susceptible to cholesterol depletion and chilling. Mol. Biol. Cell *18*, 2112–2122.

Flanagan, M.E., Abramite, J.A., Anderson, D.P., Aulabaugh, A., Dahal, U.P., Gilbert, A.M., Li, C., Montgomery, J., Oppenheimer, S.R., Ryder, T., et al. (2014). Chemical and computational methods for the characterization of covalent reactive groups for the prospective design of irreversible inhibitors. J. Med. Chem. *57*, 10072–10079.

Floppe, N., and Nilsson, L. (2007). Stabilization of the catalytic thiolate in a mammalian glutaredoxin: structure, dynamics and electrostatics of reduced pig glutaredoxin and its mutants. J. Mol. Biol. *372*, 798–816.

Fujimoto, K. (1995). Freeze-fracture replica electron microscopy combined with SDS digestion for cytochemical labeling of integral membrane proteins. J. Cell Sci. *108*, 3443–3449.

Griffin, B.A., Adams, S.R., and Tsien, R.Y. (1998). Specific covalent labeling of recombinant protein molecules inside live cells. Science *281*, 269–272.

Hainfeld, J.F., and Powell, R.D. (2000). New frontiers in gold labeling. J. Histochem. Cytochem. *48*, 471–480.

Havugimana, P.C., Hart, G.T., Nepusz, T., Yang, H., Turinsky, A.L., Li, Z., Wang, P.I., Boutz, D.R., Fong, V., Phanse, S., et al. (2012). A census of human soluble protein complexes. Cell *150*, 1068–1081.

Jao, S.-C., Enligh Oapima, S.M., Berdis, A.J., Starke, D.W., Post, C.B., and Mieya, J.J. (2006). Computational and mutational analysis of human glutaredoxin (thiotransferase): probing the molecular basis of the low pK_a of cysteine 22 and its role in catalysis. Biochemistry *45*, 4785–4796.

Kortemme, T., and Creighton, T.E. (1995). Ionisation of cysteine residues at the termini of modelα-helical peptides. Relevance to unusual thiol pK_a values in proteins of the thioredoxin family. J. Mol. Biol. *253*, 799–812.

Krall, N., da Cruz, F.P., Boutureira, O., and Bernardes, G.J.L. (2016). Site-selective protein-modification chemistry for basic biology and drug development. Nat. Chem. *8*, 103–113.

Lotze, J., Reinhardt, U., Seitz, O., and Beck-Sickinger, A.G. (2016). Peptide-tags for site-specific protein labelling in vitro and in vivo. Mol. Biosyst. *12*, 1731–1745.

Lutolf, M.P., Tirelli, N., Cerritelli, S., Cavalli, L., and Hubbell, J.A. (2001). Systematic modulation of Michael-type reactivity of thiols through the use of charged amino acids. Bioconjug. Chem. *12*, 1051–1056.

Martell, J.D., Deerinck, T.J., Sancak, Y., Poulos, T.L., Mootha, V.K., Sosinsky, G.E., Ellisman, M.H., and Ting, A.Y. (2012). Engineered ascorbate peroxidase as a genetically encoded reporter for electron microscopy. Nat. Biotechnol. *30*, 1143–1148.

Martos-Maldonado, M.C., Hjuler, C.T., Sørensen, K.K., Thygesen, M.B., Rasmussen, J.E., Villadsen, K., Midtgaard, S.R., Kol, S., Schoffelen, S., and Jensen, K.L. (2018). Selective N-terminal acylation of peptides and proteins with a Gly-His tag sequence. Nat. Commun. *9*, 3307.

Masugi-Tokita, M., and Shigemoto, R. (2007). High-resolution quantitative visualization of glutamate and GABA receptors at central synapses. Curr. Opin. Neurobiol. *17*, 287–393.

Matsuo, K., and Hamachi, I. (2017). Ligand-directed tosyl and acyl imidazole chemistry. In Chemoselective and Bioorthogonal Ligation Reactions: Concepts and Applications, *Vol. 1*, W.R. Algar, P. Dawson, and I.L. Medintz, eds., Chemoselective and Bioorthogonal Ligation Reactions: Concepts and Applications (Wiley-VCH Verlag GmbH), pp. 147–163.

Meier, C., and Beckmann, A. (2018). Freeze fracture: new avenues for the ultrastructural analysis of cells in vitro. Histochem. Cell Biol. *149*, 3–13.

Miki, T., Kaufmann, W.A., Malagon, G., Gomez, L., Tabuchi, K., Watanabe, M., Shigemoto, R., and Marty, A. (2017). Numbers of presynaptic Ca^{2+} channel clusters match those of functionally defined vesicular docking sites in single central synapses. Proc. Natl. Acad. Sci. U S A *114*, E5246–E5255.

Nonaka, H., Fujishima, S., Uchinomiya, S., Ojida, A., and Hamachi, I. (2010). Selective covalent labeling of tag-fused GPCR proteins on live cell surface with a synthetic probe for their functional analysis. J. Am. Chem. Soc. *132*, 9301–9309.

Ramil, C.P., An, P., Yu, Z., and Lin, Q. (2016). Sequence-specific 2-cyanobenzothiazole ligation. J. Am. Chem. Soc. *138*, 5499–5502.

Robertson, J.D. (1958). The cell membrane concept,. J. Physiol. (London) *140*, 58–59.

Schneider, A.F.L., and Hackenberger, C.P.R. (2017). Fluorescent labelling in living cells. Curr. Opin. Biotechnol. *48*, 61–68.

Shu, X., Lev-Ram, V., Deerinck, T.J., Qi, Y., Ramko, E.B., Davidson, M.W., Jin, Y., Ellisman, M.H., and Tsien, R.Y. (2011). A genetically encoded tag for correlated light and electron microscopy of intact cells, tissues, and organisms. PLoS Biol. *9*, e1001041.

Singh, J., Petter, R.C., and Kluge, A.F. (2010). Targeted covalent drugs of the kinase family. Curr. Opin. Chem. Biol. *14*, 475–480.

Srihari, S., Yong, C.H., Patil, A., and Wong, L. (2015). Methods for protein complex prediction and their contribution towards understanding the organization, function and dynamics of complex. FEBS Lett. *589*, 2590–2602.

Uchinomiya, S., Nonaka, H., Wakayama, S., Ojida, A., and Hamachi, I. (2013). In-cell covalent labeling of reactive his-tag fused proteins. Chem. Commun. (Camb.) *49*, 5022–5024.

Uchinomiya, S., Ojida, A., and Hamachi, I. (2014). Peptide tag/probe pairs based on the coordination chemistry for protein labeling. Inorg. Chem. *53*, 1816–1823.

Walper, S.A., Turner, K.B., and Medintz, I.L. (2017). Bioorthogonal labeling of cellular proteins by enzymatic and related mechanisms. In Chemoselective and Bioorthogonal Ligation Reactions: Concepts and Applications, *Vol. 2*Chemoselective and Bioorthogonal Ligation Reactions: Concepts and Applications (Wiley-VCH Verlag GmbH), pp. 165–230.

Wissner, A., Overbeek, E., Reich, M.F., Floyd, M.B., Johnson, B.D., Mamuya, N., Rosfjord, E.C., Discafani, C., Davis, R., Shi, X., et al. (2003). Synthesis and structure−activity relationships of 6,7-disubstituted 4-anilinoquinoline-3-carbonitriles. the design of an orally active, irreversible inhibitor of the tyrosine kinase activity of the epidermal growth factor receptor (EGFR) and the human epidermal growth factor receptor-2 (HER-2). J. Med. Chem. *46*, 49–63.

Xue, L., Karpenko, L.A., Hiblot, J., and Johnsson, K. (2015). Imaging and manipulating proteins in living cells through covalent labeling. Nat. Chem. Biol. *11*, 917–923.

Zhang, C., Welborn, M., Zhu, T., Yang, N.J., Santos, M.S., Voolhis, T.V., and Pentelute, B.L. (2016). π-clamp-mediated cysteine conjugation. Nat. Chem. *8*, 120–128.

ISCI, Volume *22*

Supplemental Information

Electron Microscopic Detection of Single Membrane Proteins by a Specific Chemical Labeling

Shigekazu Tabata, Marijo Jevtic, Nobutaka Kurashige, Hirokazu Fuchida, Munetsugu Kido, Kazushi Tani, Naoki Zenmyo, Shohei Uchinomiya, Harumi Harada, Makoto Itakura, Itaru Hamachi, Ryuichi Shigemoto, and Akio Ojida

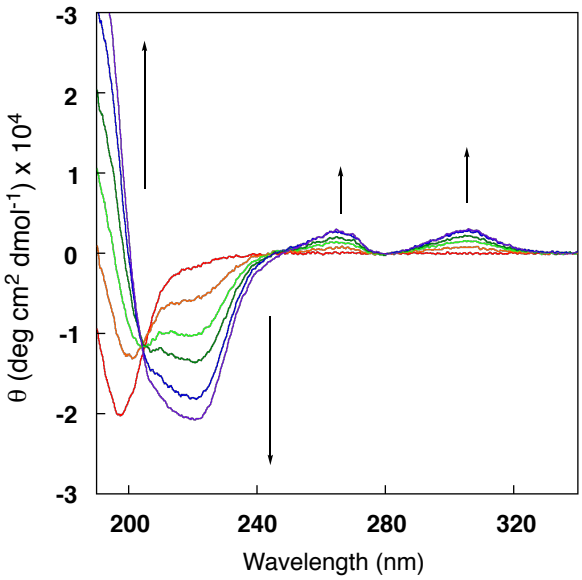

Figure S1. CD spectral change of peptide-**a** upon the addition of **2**-4Zn(II), Related to Figure 2. Measurement conditions: [peptide-**a**] = 50 μM, [**2**-4Zn(II)] = 0, 10, 20, 30, 40, and 50 μM, 10 mM borate buffer, pH 8.0, 25 ℃.

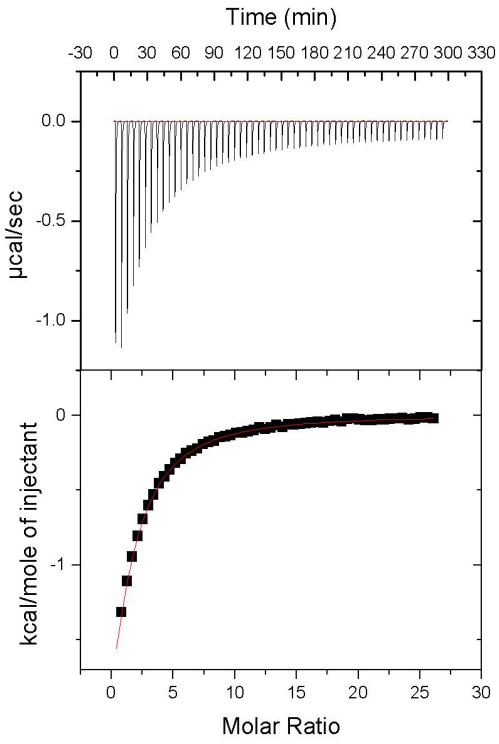

n	0.97 ± 0.06
K_{app} (M^{-1})	7.04 ± 0.15 x 10^3
ΔH (kcal/mol)	-6.67 ± 0.46
$T\Delta S$ (kcal/mol)	-1.41

Figure S2. ITC titration curve (upper) and processed data (lower) of **1**-2Zn(II) with peptide-**c** (Ac-DAAAD-NH_2), Related to Figure 2. [**1**-2Zn(II)] = 50 µM, [peptide-**c**] = 6 mM (5 µL × 48 injections), 50 mM HEPES, 100 mM NaCl, pH 7.2, 25°C.

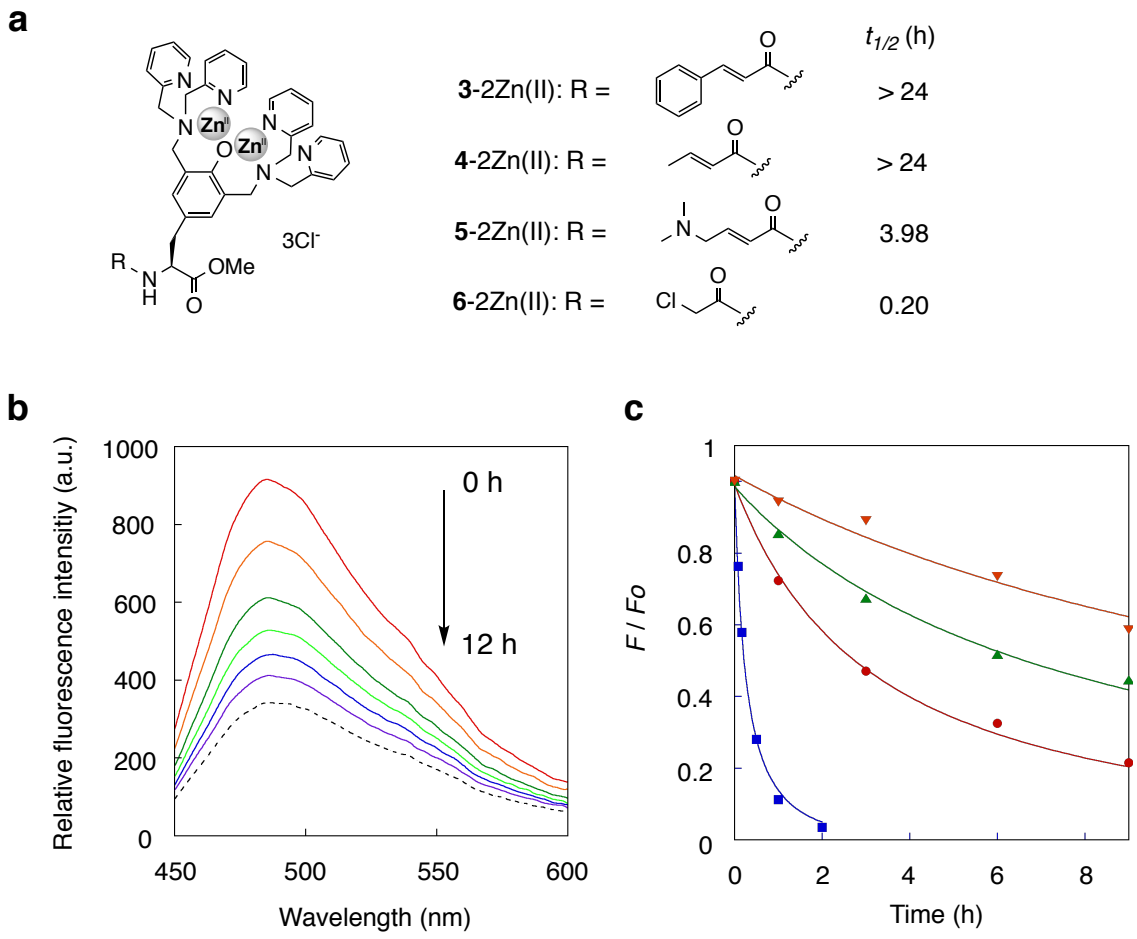

Figure S3. Evaluation of the reactivity of the zinc complexes with peptide-**g**, Related to Table 2. (a) Structures of the zinc complexes and their reaction half-time ($t_{1/2}$, h) with peptide-**g**. (b) Fluorescence intensity change of the solution containing peptide-**g** and **5**-2Zn(II) upon treatment with mCBI (reaction time: 0, 1, 3, 6, 9, and 12 h, from the upper to lower trace). The dashed line indicates the fluorescence of mCBI in the absence of peptide-**g**. Measurement conditions: [peptide-**g**] = 50 μM, [probe] = 100 μM, 50 mM HEPES, 100 mM NaCl, pH 7.2, 37 °C. (c) Plot of fluorescence intensity change for the selected reaction pairs: peptide-**g** and **7**-4Zn(II) (●), peptide-**g** and **8**-4Zn(II) (▼), peptide-**k** and **9**-4Zn(II) (■), and peptide-**i** and **7**-4Zn(II) (▲). Measurement conditions: [peptide] = 50 μM, [probe] = 60 μM, 50 mM HEPES, 100 mM NaCl, pH 7.2, 37 °C.

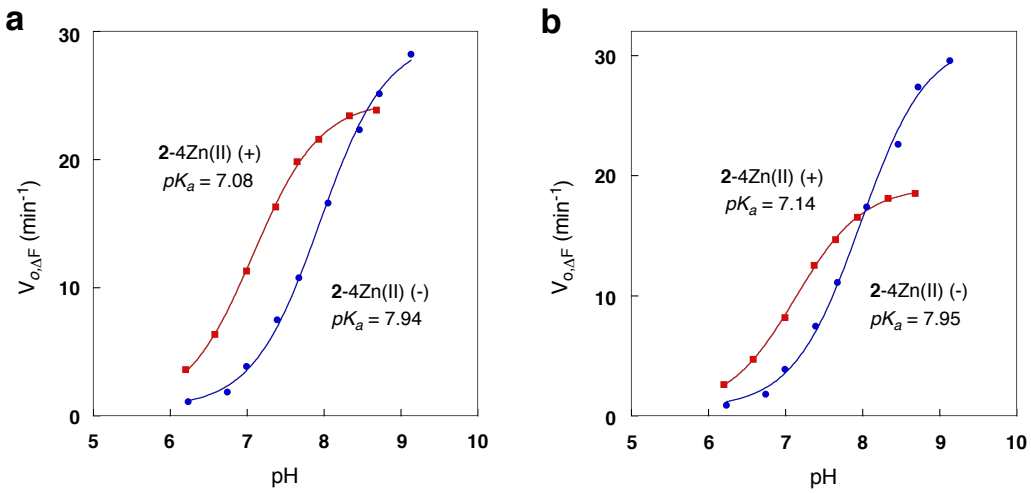

Figure S4. pH-dependent reaction rate profiles of peptide-**j (a)** and peptide-**k** (**b**) with mCBI in the presence and absence of **2**-4Zn(II), Related to Table 2. pK_a values were evaluated by applying non-linear curve fitting analysis according to Henderson-Hasselbalch equation.

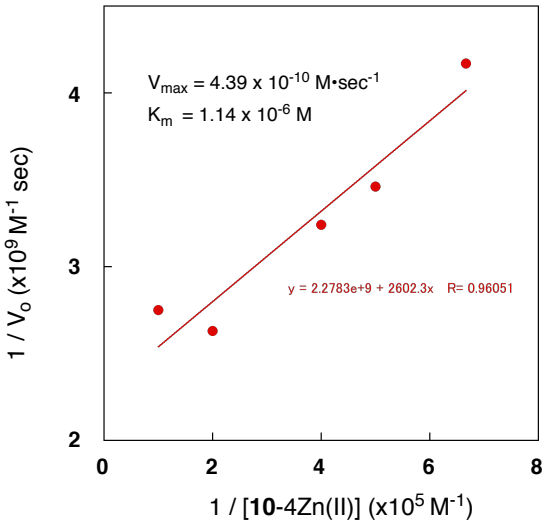

Figure S5. Second-order rate analysis of the labeling reaction of helixD2-tag fused MBP protein with **10**-4Zn(II), Related to Figure 3. The data was analyzed by double reciprocal Lineweaver-Burk plot between the probe concentration (1/[**10**-4Zn(II)]) and initial reaction rate (1/V_o).

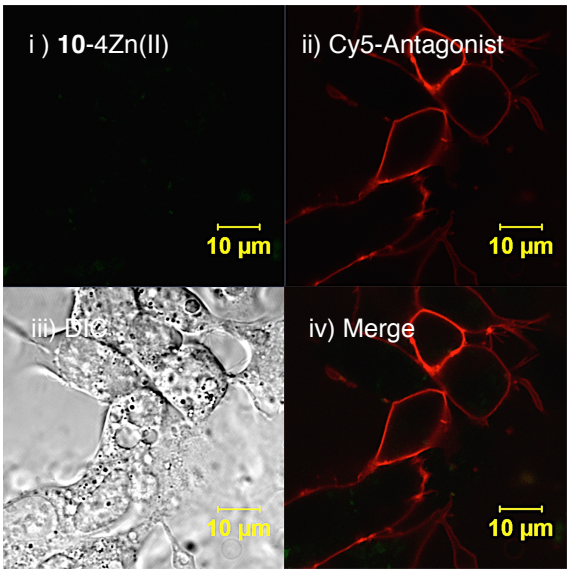

Figure S6. Fluorescence imaging of HEK293 cells expressing helixD2-tag fused B2R upon the labeling with **10**-4Zn(II) in the presence of 1 mM pyrophosphate (PPi), Related to Figure 3. Labeling conditions: [**10**-4Zn(II)] = 4 μM, HEPES-buffered saline, pH 7.4, 37 °C, 30 min.

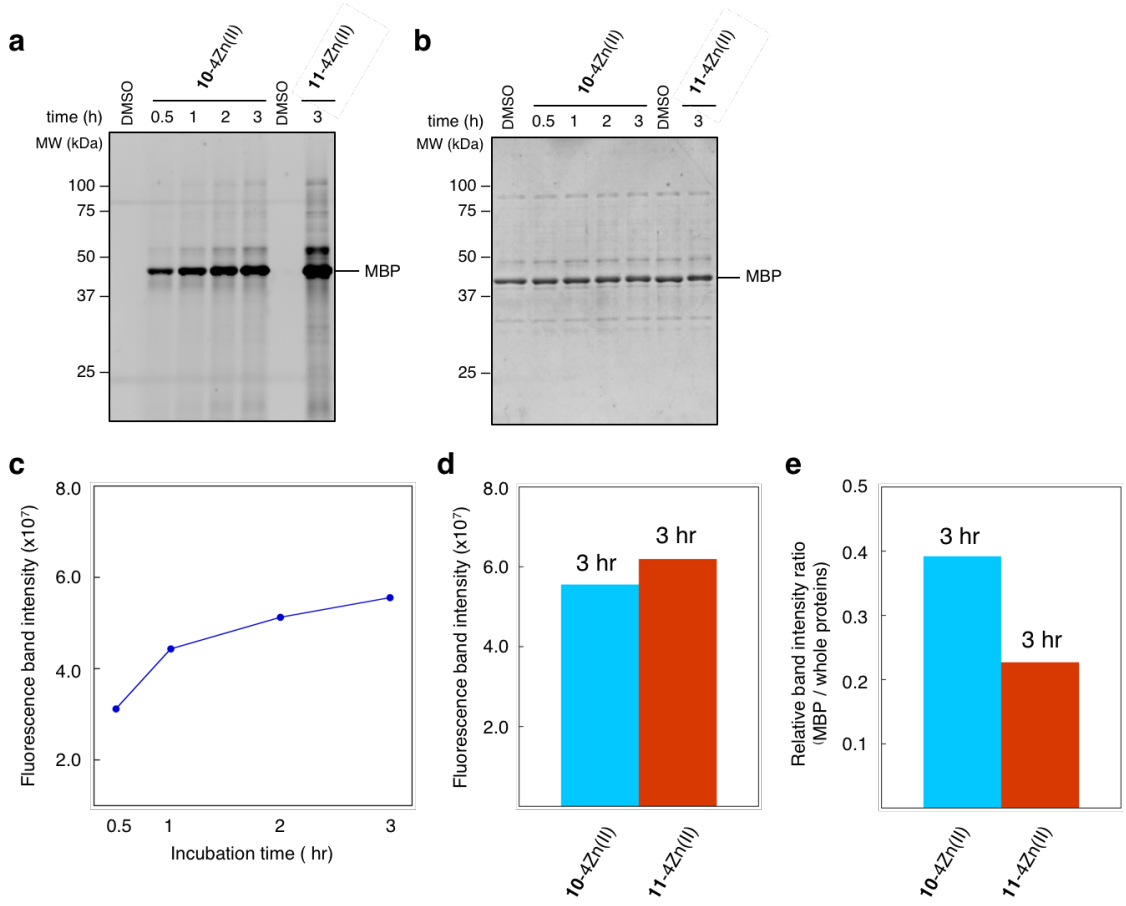

Figure S7. Evaluation of non-specific labeling activity of the probes in E.coli lysate, Related to Figure 3. (a) In-gel fluorescence analysis of helixD2-MBP labeling by **10**-4Zn(II) and **11**-4Zn(I) in the presence of E.coli lysate. (b) CBB image of the gel shown in (a). (c) time-trace plot of the band intensity of helixD2-MBP labeled by **10**-4Zn(II). (d) Comparison of band intensity of helixD2-MBP labeled by **10**-4Zn(II) or **11**-4Zn(II) at 3 hr. (e) Comparison of relative band intensity ratio of helixD2-MBP against whole proteins labeled by **10**-4Zn(II) or **11**-4Zn(II). Note that the relative band intensity ratio of **10**-4Zn(II) is significantly higher than that of **11**-4Zn(II) as shown in (e), while the band intensity of helixD2-MBP labeled by **10**-4Zn(II) was not greatly different from that by **11**-4Zn(II) as shown in (d).

]

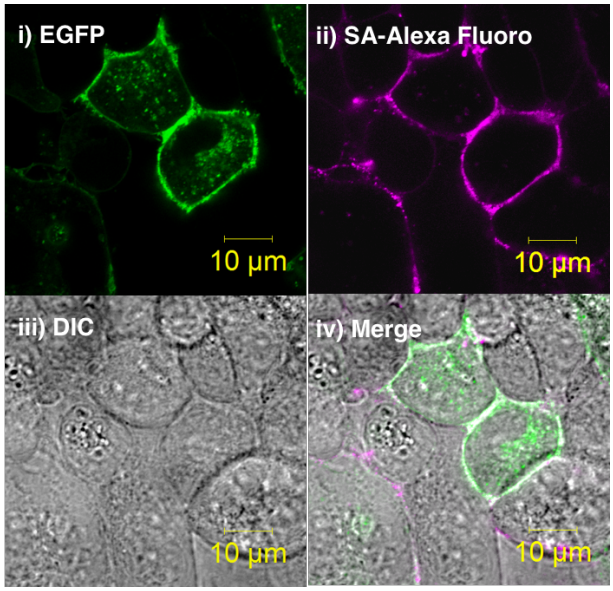

Figure S8. Fluorescence imaging of helixD2-tag fused B2R upon the labeling with **12**-4Zn(II), Related to Figure 4. The labeling reaction was conducted by the same procedure as described for **10**-4Zn(II). After the labeling, the cells were treated with Alexa Fluoro 633-conjugated streptavidin (5 μg/mL in PBS) and subjected to fluorescence imaging.

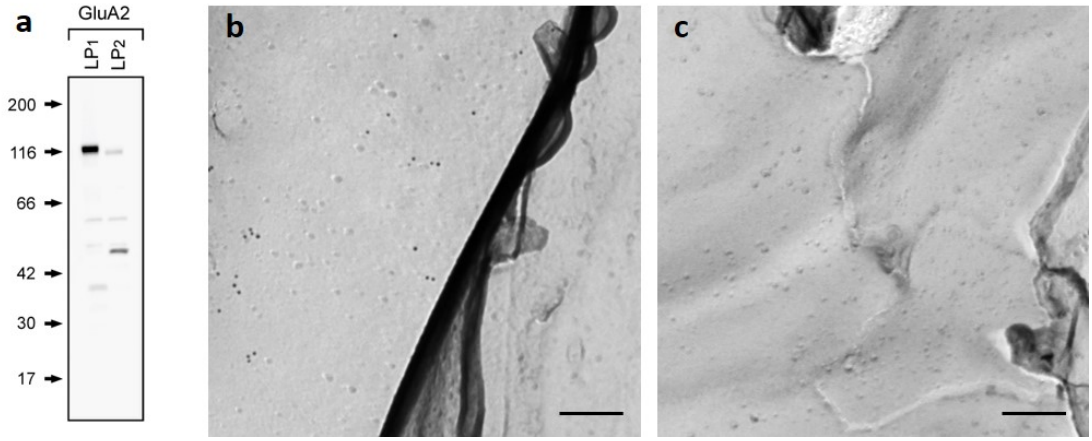

Figure S9. Characterization of rabbit polyclonal antibody for GluA2 AMPA receptor subunit raised against a synthetic peptide (CERDKVNDIVDQVITIGKH), Related to Figure 5. (a) Western-blotting analysis to characterize specificity of the anti-GluA2 antibody. The antibody recognizes a broad band (100-120 kDa) on immunoblots of rat brain LP1 (crude synaptic plasma membrane) and a weak band on LP2 (synaptic vesicle). Subcellular fractionation was performed as described (Yamamori *et al.*, 2011). (b and c) EM images of replicas prepared from GluA2-transfected (b) and non-transfected (c) HEK cells labeled with the anti-GluA2 antibody followed by 10 nm gold-conjugated secondary antibody. Scale bars, 200 nm.

Transparent Methods

Circular Dichroism (CD) Measurement. Aqueous solution of the zinc complex was added to a solution of the peptide (50 μM) in 10 mM borate buffer (pH 8.0). CD spectrum was measured at rt in a quartz cell (0.1 cm path length) using JASCO J-720W spectropolarimeter. The data of each sample was collected by 5 scans (scan range; 350 ~ 190 nm, scan speed; 50 nm•min^{-1}) and averaged to give CD spectrum.

Isothermal Titration Calorimetry (ITC) Measurement. ITC titration was performed with isothermal titration calorimeter (Malvern) at 298 K. Solution of peptide-**c** (6.0 mM) in buffer solution (50 mM HEPES, 100 mM NaCl, pH 7.2) was injected stepwise (5 μL x 48 times) to solution of **1**-2Zn(II) (50 μM) in the same solvent system. The measured heat flow was recorded as function of time and converted into enthalpies (ΔH) by integration of the appropriate reaction peaks. Dilution effects were corrected by subtracting feat flow of blank experiment upon injection of the HEPES buffer under identical experimental conditions. The binding parameters (Kapp, ΔH, ΔS, n) were evaluated by applying one site model using the software Origin (Malvern).

Evaluation of Binding Constant. In a quartz cell, peptide-**b** (0.05 μM, final concentration) dissolved in 3 mL buffer (50 mM HEPES 100 mM NaCl, pH 7.2) was titrated with a freshly prepared aqueous solution of 2-4Zn(II) using a micro syringe at 25 °C. The fluorescence spectrum was measured (λ_{ex} = 410 nm) using Perkin-Elmer LS55 spectrometer at each titration point. The change of the fluorescence intensity at 448 nm was analyzed by nonlinear least-square curve-fitting method to yield the apparent binding constant (K_{app}, M^{-1}).

Kinetic Analysis of Nucleophilic Reaction of Peptide with mCBI. 10 μL of stock solution of mCBI (10 mM in DMSO) was added to a solution of peptide (4 μM) in 0.8 mL of buffer (50 mM HEPES 100 mM NaCl, pH 7.2, degassed under reduced pressure and charged with nitrogen before use) in the presence or absence of 2-4Zn(II) (14 μM). The fluorescence emission at 486 nm was continuously monitored by Perkin-Elmer LS55 spectrometer ((λ_{ex} = 396 nm) at 37 °C. The emission change was analyzed by nonlinear least-square curve-fitting method to yield the first-order reaction constant (k, sec^{-1}). For evaluation of pK_a value of the cysteine residue, initial reaction rate of fluorescence change ($V_{o,\ \Delta F}$, min^{-1}) were measured under the different pH

conditions in universal pH buffer (5 mM CHES-5 mM HEPES-5 mM MES, degassed under reduced pressure and charged with nitrogen before use) at 37 °C. The change of the initial rate over the pH range was analyzed by nonlinear curve-fitting method according to Henderson-Hasselbalch equation to yield pK_a value.

Kinetic Analysis of Cysteine Conjugation of Peptide with Zinc Complex. Peptide (50 μM) and zinc complex (60 μM) was dissolved in 200 □L of buffer solution (50 mM HEPES 100 mM NaCl, pH 7.2, degassed under reduced pressure and charged with nitrogen before use) and incubated at 37 °C in a plastic tube. Aliquot of the solution (20 μL) was sampled at appropriate times and mixed with 6 μL of inorganic pyrophosphate solution (10 mM in water) to quench the reaction followed by being kept at -20 °C. The thawed samples were mixed with 4 μL of mCBI (5 mM in DMSO) and incubated at 37 °C for 1 h in a dark. The solution (18μL) was diluted with a 582 μL of buffer solution (50 mM HEPES 100 mM NaCl, pH 7.2), and the fluorescence was measured (λ_{ex} = 396 nm) in a quartz cell using Perkin-Elmer LS55 spectrometer. The fluorescence change (λ_{em} = 486 nm) was analyzed by nonlinear least-square curve-fitting method according to second-order equation to yield half-reaction time ($t_{1/2}$, h).

Fluorescence Detection of Covalent Labeling of Tag-fused MBP. A solution of helixD2-tag-fused MBP (1 μM) or CH6 tag-fused MBP (1 μM) in 50 mM HEPES, 100 mM NaCl, 20 μM TCEP, pH 7.2 (degassed under reduced pressure and charged with nitrogen before use) was mixed with **10**-4Zn(II) (10 μM, final concentration), and the mixture was incubated in a plastic tube at 37 °C. Aliquot of the solution (8 μL) was sampled at the appropriate times and mixed with 2 μL inorganic pyrophosphate solution (10 mM in water) followed by being kept at -20 °C. After thawing, the samples were mixed with 5x sampling buffer and heated at 95 °C for 2 min followed by being applied to SDS-PAGE. In-gel fluorescence and CBB analyses were performed with LAS-4000 lumino image analyzer (FUJIFILM) by EPI (460 nm excitation, Y515Di filter) and DIA-W mode, respectively.

Cell Culture and B2R Expression in HEK293 Cells. HEK293 cells were cultured in high glucose DMEM supplemented with 10% fetal bovine serum (FBS), penicillin (100 units/mL), streptomycin (100 μg/mL) and amphotericin B (250 ng/mL). Cells were maintained at 37 ºC in humidified atmosphere of 5% CO_2 in air. Subculture was performed every 3-4 days from subconfluent (< 80%) cultures using trypsin-EDTA solution. Transfection of the expression

vector for B2R was carried out in a 35 mm glass-bottomed dish (Iwaki) using Lipofectamine LTX (Invitrogen) according to the general procedure. The cells were subjected to labeling experiment after 48 h of the transfection.

Fluorescence Imaging of Tag-fused B2R. In a glass bottom dish, HEK293 cells (~ 1 x 10^6) transiently expressing helixD2-tag fused B2R or CH6 tag-fused B2R were incubated in non-serum Dulbecco's modified Eagle medium (DMEM) containing 2-deoxy-D-glucose (10mM) and sodium azide (6 mM) for 30 min at 37 °C in CO_2 incubator. After removal of DMEM, cells were treated with TCEP (1 mM) for 10 min at rt in 1 mL HEPES-buffered saline (HBS, containing 107 mM NaCl, 6 mM KCl, 1.2 mM $MgSO_4$, 2 mM $CaCl_2$, 11.5 mM glucose, 10 mM 2-deoxy-D-glucose, 6 mM sodium azide 20 mM HEPES, adjusted to pH 7.4 with NaOH). TCEP solution was removed and then cells were treated with **10**-4Zn(II) (4 μM, final concentration) for 30 min in HBS containing 2-deoxy-D-glucose (10 mM) and sodium azide (6 mM) at 37 °C. Cells were washed three times with HBS containing 2 mM pyrophosphate (PPi) (1 mL) to remove unreacted **10**-4Zn(II). HBS containing Cy5-appended B2R antagonist peptide (0.4 μM) was added and cells were analyzed by confocal laser scanning microscope (Zeiss, LSM700) using appropriate laser and emission filter settings for Oregon Green 488 (λ_{ex} =488 nm, λ_{em} = 490-555 nm) and Cy5 (λ_{ex} = 639 nm, λ_{em} > 640 nm).

Evaluation of Non-specific Labeling Property of Probe. In a glass bottom dish, HEK293 cells (~ 1 x 10^6) were incubated in non-serum DMEM containing 2-deoxy-D-glucose (10mM) and sodium azide (6 mM) for 30 min at 37 °C in a CO_2 incubator. After removal of DMEM, cells were treated with TCEP (1 mM) for 10 min at rt in 1 mL HEPES-buffered saline. TCEP solution was removed and then cells were treated with **10**-4Zn(II) or **11**-4Zn(II) (4 μM, final concentration) for 10 or 30 min in HBS containing 2-deoxy-D-glucose (10 mM) and sodium azide (6 mM) at 37 °C. After washing three times with HBS containing 2 mM PPi (1 mL), the cells were fixed by treatment with PBS (100 μL) containing 4% paraformaldehyde, 0.2% glutaraldehyde, and 2 mM PPi for 10 min with gentle shaking (80 rpm) at rt. The fixed cells were washed three times with HBS containing 0.1% Triton-X and 2 mM pyrophosphate (PPi) (1 mL) by gentle shaking (80 rpm) for 10 min at rt. The cells were immersed in HBS (100 μL) and the fluorescence on the cell surfaces were detected by confocal laser scanning microscope (Leica, TCS SP8) equipped with HyD detector with a high laser power (1%) for Oregon Green 488 (λ_{ex}

=488 nm). The fluorescence image was analyzed by ImageJ software (National Institutes of Health) to obtain the fluorescence intensity per area on the cell surface.

EM Detection of B2R in Freeze-fracture Replicas. HEK293T cells (ca. 2×10^7 cells) transiently expressing helixD2-B2R-EGFP, GluA2 (for negative control) or co-expressing helixD2-B2R-EGFP and GluA2 were washed with HEPES-buffered saline (HBS), and treated with 2 mM TCEP in HBS (1 mL) for 10 min at 37 °C. After removal of TCEP solution, the cells were treated with 3 μM **12**-4Zn(II) in HBS for 30 min at 37 °C, or with 3 μM **13**-4Zn(II) in HBS for 2 h at 37 °C. After washing with HBS containing 2 mM PPi, the cells labeled with **12**-4Zn(II) were incubated with 1.4-nm gold particle-conjugated streptavidin (Nanoprobes) for 1 h at 37 °C. For estimation of chemical labeling density in unfixed cells, cells were fixed after chemical labeling (after washing out the 13-4Zn(II) with PPi) and for estimation of chemical labeling density in fixed cells, fixation was performed before chemical labeling (before HBS washing). Fixation was done with 2% paraformaldehyde in phosphate-buffered saline (PBS) for 15 min at RT. The cells were harvested by scraping, collected by centrifugation (100g, 5 min), and the cell pellet was sandwiched between gold carriers for high-pressure freezing (HPM010, Bal-Tec). The frozen pellet was then fractured into two parts at –120 °C and replicated by depositions of 30 nm carbon layer using freeze-fracture replica machine (BAF 060, Bal-Tec). After thawing, the replicas were washed with 2.5% SDS, 20% sucrose, and 15 mM Tris-HCl (pH 8.3) under the following conditions: 48 h at 60 °C for labeling with **13**-4Zn(II); 3 d at 60 °C for labeling of pre-fixed cells with **12**-4Zn(II); and 18 h at 60 °C for labeling with **12**-4Zn(II).

For EM detection of 1.4-nm gold particle-conjugated streptavidin, the replicas were treated with reagents from a silver intensification kit (HQ Silver, Nanoprobes). For immunolabeling, the replicas were treated with mouse anti-GFP (CLONTECH), rabbit anti-FLAG (Sigma-Aldrich) or rabbit anti-GluA2 antibodies (Figure S9) for 48 h at 15 °C, followed by staining with anti-mouse secondary antibody conjugated with 5-nm gold particles or anti-rabbit secondary antibody conjugated with 10-nm gold particles (British Biocell International). The silver-intensified replicas were analyzed by EM using Tecnai 10/12 transmission electron microscope (FEI); those without silver intensification were analyzed by JEM-2800 scanning transmission electron microscope (JEOL) in dark field mode. For quantitative analysis of particle distribution, we used GPDQ software (Wickman *et al.*, 2018) to calculate the density and NND of particles, particle number per cluster, and cluster area. For the definition of clusters of particles, we used 3 particles as a minimum number and mean + 2SD (Miki *et al.*, 2017; Wickman *et al.*, 2018) of

fitted peaks of NND (Figure 5I) as a maximum distance allowed (6 + 3×2 = 12 nm for chemical labeling, 22 + 10×2 = 42 nm for immunolabeling).

EM Detection of B2R in Embedded Ultrathin Sections. HEK293 cells (*ca.* 2×10^7 cells) transiently expressing helixD2-B2R-EGFP cultured on a coverslip were treated with 2 mM TCEP in HBS for 10 min at 37 °C. After removal of the solution, the cells were treated with 3 μM **13**-4Zn(II) for 2 h at 37 °C, and washed with 2 mM PPi in HBS. The cells were then fixed in PBS containing 4% paraformaldehyde and 0.05% glutaraldehyde for 10 min at rt. After 3-6 min silver intensification, the cells were treated with 0.2% OsO_4 in PBS for 20 min, counterstained with 0.25% uranyl acetate overnight at 4 °C, dehydrated in ascending series of EtOH and propylene oxide, and embedded in Durcupan (Sigma-Aldrich). Ultrathin sections (70-μm thick) prepared using ultramicrotome (Leica Ultracut UCT, Leica) were counterstained with lead citrate and uranyl acetate, and analyzed by Tecnai 10 transmission electron microscope (FEI). For immunolabeling of the FLAG tag, HEK293 cells were fixed by 4% paraformaldehyde and 0.05% glutaraldehyde in PBS for 10 min at rt. After blocking with 10% normal goat serum and 2% bovine serum albumin in Tris-buffered saline (TBS), the cells were treated with anti-FLAG antibody (Sigma-Aldrich) followed by anti-mouse secondary antibody conjugated with 1.4-nm gold particles (Nanoprobes). After 3-6 min silver intensification, the cells were treated, sectioned and observed in the same way as described above. To measure the distance between gold particles and cell membrane, we first tilted the ultrathin sections to obtain perpendicular views of lipid bilayer (Figure 6B and 6D). We discarded the particles if it was not possible to obtain perpendicular views. Then, the distance between the center of silver-intensified gold particles and the midpoint of plasma membrane was determined by ImageJ v1.51 software (National Institutes of Health).

Construction of expression-vectors of the tag-fused maltose binding protein (MBP)

DNA encoding helixD2-tag (KKCPYSAADAAADAAADAAAD) was introduced into the pMAL-c2X vector (New England BioLabs) encoding D4-tag fused MBP (Nonaka *et al.*, 2010) by inverse polymerase chain reaction (PCR). After digestion of the template plasmid by the treatment with *Dpn* I, 5'-termini of the PCR product were phosphorylated by T4 polynucleotide kinase and then cyclized by DNA ligase to give the vector encoding helixD2-tag fused MBP. The DNA sequence of the vectors was confirmed by 3130xl Genetic Analyzer (Applied Biosystems).

Expression and purification of tag-fused MBP

pMAL-c2X vector encoding helixD2-tag fused MBP was transformed into T7 Expression *lysY/I*^{q} competent *E. coli* (New England BioLabs). Single colony was cultured at 37 °C in 2YT media (200 mL) containing ampicillin (100 mg/L) at 37 °C until optical density (OD) at 600 nm increased to 0.6. and further grown at 37 °C for 6 h with IPTG induction (1 mM final conc.). Cells were spun down for 10 min at 13,500 rpm and re-suspended in equilibrium buffer (20 mM Tris–HCl, 200 mM NaCl, 1mM EDTA, 1mM DTT, pH 8.0) and then lysed by sonication (150 shots x 2) on ice. Insoluble materials were removed by centrifugation (13,500 rpm, 10 min) and supernatant was applied to a MBPTrap affinity column (GE Healthcare). Column was washed with equilibrium buffer (x2) and then MBP was eluted by elusion buffer (20 mM Tris–HCl, 200 mM NaCl, 10 mM maltose, pH 8.0). Purity of MBP in fractions was checked by SDS-PAGE. Concentration of purified MBP was determined by the UV absorbance at 280 nm using the calculated extinction coefficient (ε_{280nm} = 69,330 $M^{-1}cm^{-1}$). MBP solution was kept at 4 °C in the presence of 1 mM TCEP.

Construction of vectors of tag-fused B2R receptor

DNA encoding helixD2-tag (KKCPYSAADAAADAAADAAAD) or CH6 tag inserted into pCIneo plasmid encoding α7-D4-B2R vector (Nonaka *et al.*, 2010) by inverse polymerase chain reaction (PCR). After digestion of template plasmid by the treatment with *Dpn* I, 5'-termini of the PCR product were phosphorylated by T4 polynucleotide kinase and then cyclized by DNA ligase to give the vector encoding α7-helixD4-B2R or α7-CH6-B2R. DNA sequences were confirmed by 3130xl Genetic Analyzer (Applied Biosystems).

Solid-Phase Peptide Synthesis

Peptides except for peptide-**c** were synthesized by solid-phase peptide synthesis using standard Fmoc-based coupling chemistry. Coupling reactions (0.2 mmol scale) were performed using 4 equiv of amino acid, 4 equiv of HOBt and 4 equiv of HBTU on Rink Amide MBHA Resin LL (0.2 mmol, 0.38 mmol/g, Merck Millipore). *N*-terminal was acetylated by treatment with 20 equiv of Ac_2O in NMP. Peptide cleavage and deprotection were carried out by treatment of resin with TFA / H_2O / triisopropylsilane (95 : 2.5 : 2.5) for 3 h at rt. The crude peptide was collected by precipitation in *tert*-butyl methyl ether and purified by reverse-phase HPLC (column; YMC-pack ODS-A, 20 x 250 mm) using CH_3CN (0.1% TFA) / H_2O (0.1% TFA) solvent system with a linear gradient mode. Typical HPLC conditions are as follows; 5 / 95 (0 min) →5 / 95 (10 min) → 40 / 60 (50 min), flow rate 9.9 mL/min, UV detection at 220 nm. Purified peptide was lyophilized and stocked in a refrigerator (-30 °C).

MALDI-TOF-MS analysis (CHCA)

peptide-**a**: calcd for $C_{57}H_{84}N_{16}O_{25}$ (MW; 1392.6), found 1416.3 $[M+Na]^+$.

peptide-**b1**[a]: calcd for $C_{54}H_{87}N_{17}O_{24}$ (MW; 1357.6), found 1358.7 $[M+H]^+$.

peptide-**d**: calcd for $C_{68}H_{102}N_{20}O_{29}S$ (MW; 1694.7), found 1694.3 $[M]^+$.

peptide-**e**: calcd for $C_{69}H_{102}N_{20}O_{29}S$ (MW; 1706.7), found 1706.8 $[M]^+$.

peptide-**f**: calcd for $C_{70}H_{104}N_{20}O_{29}S$ (MW; 1720.7), found 1719.8 $[M-H]^-$.

peptide-**g**: calcd for $C_{77}H_{120}N_{22}O_{30}S$ (MW; 1864.8), found 1864.2 $[M-H]^-$.

peptide-**h**: calcd for $C_{77}H_{120}N_{26}O_{30}S$ (MW; 1920.8), found 1920.2 $[M-H]^-$.

peptide-**i**: calcd for $C_{68}H_{95}N_{19}O_{36}S$ (MW; 1785.6), found 1783.1 $[M-H]^-$.

peptide-**j**: calcd for $C_{80}H_{125}N_{23}O_{31}S$ (MW; 1935.9), found 1937.0 $[M]^-$.

peptide-**k**: calcd for $C_{83}H_{130}N_{24}O_{32}S$ (MW; 2006.9), found 2005.5. $[M-H]^-$.

[a)] peptide-**b1** is a peptide that lacks 7-hydroxycumarin from peptide-**b**.

Conjugation of peptide-b1 with 7-hydroxycumarine

A solution of the peptide-**b1** (3 mg, 2.21 μmol), 7-hydroxycumarine succinimidyl ester (3.3 mg, 11.1 μmol) and DIEA (438 μL, 1.16 mmol) in dry DMF (2 mL) was stirred overnight at rt. H_2O (1.5 mL) was added, the solution was stirred for 1 h at rt. Purification was conducted by HPLC (column; YMC-Actus Triart C18, 20 x 250 mm) using CH_3CN (0.1% TFA) / H_2O (0.1%

TFA) solvent system with a linear gradient mode. The collected fractions were lyophilized to give peptide-**b**.

HPLC conditions: column; YMC-Actus Triart C18, 250 x 20 mm, mobile phase; CH_3CN (containing 0.1% TFA) / H_2O (containing 0.1% TFA) = 5 / 95(0-10 min) → 60 / 40 (linear gradient over 50 min), MALDI-TOF-MS: calcd for $C_{64}H_{91}N_{17}O_{28}$ 1545.6, found 1544.5 $[M-H]^-$.

General Materials and Methods for Organic Synthesis

Unless otherwise noted, chemical reagents were purchased from commercial suppliers (Tokyo Chemical Industry (TCI), Wako Pure Chemical Industries, Watanabe Chemical Industries, and Sigma-Aldrich) and used without further purification. ^{1}H-NMR spectra were recorded using Varian UNITY-400 (400 MHz) spectrometer, and chemical shifts (δ, ppm) were referenced to residual solvent peak. ESI and MALDI-TOF mass spectra were measured using Bruker micrOTOF II and Bruker autoflex III spectrometer, respectively. HPLC purification was conducted with Hitachi L-7100. Compound **6**, **15** and **18** were synthesized according to the previous report (Nonaka *et al.*, 2010).

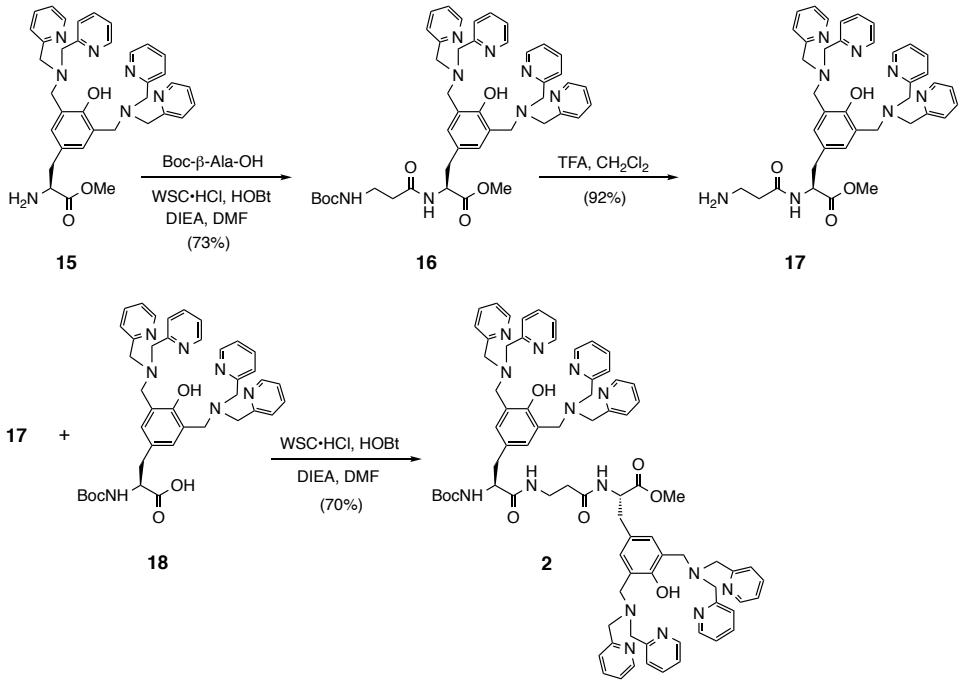

Synthesis of **16**

To a solution of Boc-βAla-OH (185 mg, 0.98 mmol) in dry DMF (5 mL) was added WSCI·HCl (188 mg, 0.98 mmol), HOBt·H_2O (150 mg, 0.98 mmol), DIEA (391 μL, 2.4 mmol) and **15** (433 mg, 0.70 mmol). The solution was stirred overnight at rt. After dilution with AcOEt, the mixture was washed with saturated $NaHCO_3$ and brine followed by drying over Na_2SO_4. After removal of the solvent by evaporation, the residue was purified by column chromatography on SiO_2 ($CHCl_3$: MeOH : NH_3 = 400 : 10 : 1 → 300 : 10 : 1) to give **16** (410 mg, 73%) as a colorless amorphous powder.

^{1}H-NMR(400 MHz, $CDCl_3$): δ 10.99 (1H, br), 8.50 (4H, s), 7.56 (4H, t, *J* = 7.4 Hz), 7.42 (4H, d, *J* = 7.6 Hz), 7.09 (4H, t, *J* = 5.8 Hz), 6.94 (2H, s), 6.71 (1H, d, *J* = 8.0 Hz), 5.26 (1H, br), 4.74

(1H, m), 3.83 (8H, s), 3.75 (4H, s), 3.65 (3H, s), 3.25 (2H, d, J = 5.6 Hz), 3.01 (2H, t, J = 8.8 Hz), 2.21 (2H, m), 1.37 (9H, s). ESI-TOF-MS *m/z* $[M + Na]^+$ calcd for $C_{44}H_{52}N_8O_6Na$ 811.39; Found 811.39.

Synthesis of **17**

To an ice-cooled solution of **16** (410 mg, 510 μmol) in CH_2Cl_2 (2.5 mL) was added dropwise TFA (2.5 mL) and the solution was stirred for 1 h at rt. The solvent was removed in vacuo and the residue was dissolved in H_2O. The mixture was neutralized with aq. NH_3 on ice-cooling and then extracted with CH_2Cl_2. The organic layer was washed with brine followed by drying over Na_2SO_4. The solution was concentrated by evaporation to give **17** (330 mg, 92%) as a colorless amorphous powder.

^{1}H-NMR (400 MHz, $CDCl_3$) : δ 10.90 (1H, br), 8.47 (4H, s), 8.25 (1H, br), 7.51 (4H, t, J = 7.4 Hz), 7.30 (4H, d, J = 7.6 Hz), 7.07 (4H, t, J = 6.0 Hz), 6.93 (2H, s), 4.66 (1H, br), 3.86 (4H, m), 3.65 (11H, m), 2.93 (4H, m), 2.59 (1H, br), 2.33 (1H, m). ESI-TOF-MS *m/z* $[M + Na]^+$ calcd for $C_{39}H_{45}N_8O_4Na$ 689.36; Found 689.36.

Synthesis of **2**

To a solution of **18** (430 mg, 0.61 mmol) in dry DMF (5 mL) was added WSCI•HCl (115 mg, 0.61 mmol), HOBt•H_2O (93 mg, 0.61 mmol), DIEA (246 μL, 1.41 mmol) and **17** (330 mg, 0.47 mmol). The solution was stirred overnight at rt. After dilution with AcOEt, the mixture was washed with saturated $NaHCO_3$ and brine followed by drying over Na_2SO_4. After removal of the solvent by evaporation, the residue was purified by column chromatography on SiO_2 ($CHCl_3$: MeOH : NH_3 = 300 : 10 : 1→200 : 10 : 1) to give **2** (450 mg, 70%) as a colorless amorphous powder.

^{1}H-NMR(400 MHz, $CDCl_3$): δ 10.95 (2H, br), 8.47 (8H, s), 7.56 (8H, m), 7.40 (8H, t, J = 6.4 Hz), 7.14 (1H, br), 7.04 (10H, m), 6.95 (2H, s), 5.36 (1H, br), 4.65 (1H, m), 4.23 (1H, br), 3.73 (25H, m), 3.57 (3H, s), 3.46 (1H, s), 3.16 (1H, br), 2.91 (4H, m), 2.11 (2H, m), 1.24 (9H, s). ESI-TOF-MS 1396.66 $[M + H]^+$. ^{13}C NMR (125 MHz, $CDCl_3$) δ 173.1, 172.1, 172.0, 159.1, 155.7, 155.1, 155.0, 149.0, 136.9, 130.4, 130.3, 126.5, 126.0, 124.0, 123.3, 123.3, 122.2 x 2, 79.7, 59.7, 56.4, 54.9, 54.8, 54.1, 52.3, 37.9, 36.5, 35.9, 35.8, 28.3. ESI-TOF-MS *m/z* $[M + Na]^+$ calcd for $C_{79}H_{87}N_{15}O_8Na$ 1396.68; Found 1396.66.

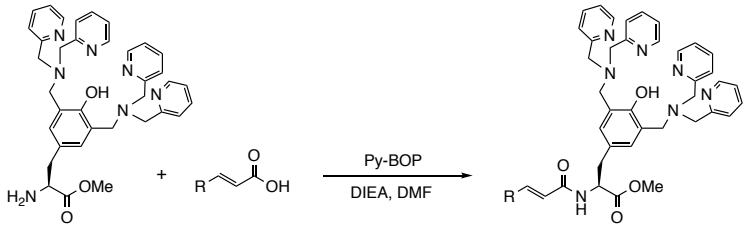

15

3: R = Ph (86%)
4: R = CH_3 (21%)
5: R = $CH_2N((CH_3)_2$ (95%)

Synthesis of **3**

To an ice-cooled solution of cinnamic acid (12 mg, 81 μmol) in dry DMF (1.5 mL) was added triethylamine (11 μL, 81 μmol), Py-BOP (36 mg, 81 μmol) and **15** (50 mg, 81 μmol). The solution was stirred for 3 h at rt. After dilution with AcOEt, the mixture was washed with saturated $NaHCO_3$ and brine followed by drying over Na_2SO_4. After removal of the solvent by evaporation, the residue was purified by column chromatography on SiO_2 ($CHCl_3$: MeOH : NH_3 = 400 : 10 : 1) to give **3** (52 mg, 86%) as a colorless amorphous powder.

^{1}H-NMR(400 MHz, DMSO-d_6): δ 10.94 (1H, s), 8.49-8.45 (5H, m), 7.68 (4H, t, *J* = 7.2 Hz), 7.44-7.32 (9H, m), 7.20 (4H, t, *J* = 6.0 Hz), 7.05 (2H, s), 6.65 (1H, d, *J* = 16 Hz), 4.6 (1H, q, *J* = 13.6 Hz, 6.4 Hz), 3.73 (8H, s), 3.64 (4H, s), 3.52 (3H, s), 2.98-2.85 (1H, m). ESI-TOF-MS *m/z* $[M + H]^+$ calcd for $C_{45}H_{46}N_7O_4$ 748.36; Found 748.38.

Synthesis of **4**

To an ice-cooled solution of crotonic acid (4.1 mg, 48 μmol) in dry DMF (1.5 mL) was added a mixture of triethylamine (6.7 μL, 48 μmol), Py-BOP (22 mg, 48 μmol) and **15** (30 mg, 48 μmol). The solution was stirred for 28 h at rt. After dilution with AcOEt, the mixture was washed with saturated $NaHCO_3$ and brine followed by drying over Na_2SO_4. After removal of the solvent by evaporation, the residue was purified by column chromatography on SiO_2 ($CHCl_3$: MeOH : NH_3 = 250 : 10 : 1) to give a pale yellow oil (24 mg). This oil was further purified by column chromatography on SiO_2 ($CHCl_3$: MeOH : NH_3 = 350 : 10 : 1) to give **4** (7 mg, 21%) as a pale yellow oil.

^{1}H-NMR(400 MHz, $CDCl_3$): δ 10.94 (1H, br), 8.52 (4H, d, *J* = 4.8 Hz), 7.60 (4H, t, *J* = 7.6 Hz), 7.44 (4H, d, *J* = 8.0 Hz), 7.11 (4H, t, *J* = 6.4 Hz), 6.97 (2H, s), 6.80-6.74 (1H, m), 6.41 (1H, d, *J* = 7.6 Hz), 4.86 (1H, q, *J* = 13.6 Hz, 7.6 Hz), 3.85 (8H, s), 3.76 (4H, s), 3.65 (3H, s), 3.05 (2H, d, *J* = 5.2 Hz), 1.68 (3H, d, *J* = 6.8 Hz). ESI-TOF-MS *m/z* $[M + H]^+$ calcd for $C_{40}H_{44}N_7O_4$ 686.34; Found 686.36.

Synthesis of **5**

To an ice cooled solution of 4-(dimethylamino)-2-butenoic acid hydrochloride (13 mg, 80 μmol) in dry DMF (1.5 mL) was added DIEA (44 μL, 240 μmol), Py-BOP (36 mg, 80 μmol) and **15** (50 mg, 80 μmol). The solution was stirred for 44 h at rt. After dilution with AcOEt, the mixture was washed with saturated $NaHCO_3$ and brine followed by drying over Na_2SO_4. After removal of the solvent by evaporation, the residue was purified by column chromatography on SiO_2 ($CHCl_3$: MeOH : NH_3 = 300 : 10 : 1→150 : 10 : 1) to give **5** (56 mg, 95%) as a pale yellow oil.

^{1}H-NMR(400 MHz, $CDCl_3$): δ 8.52 (4H, d, *J* = 4.8 Hz), 7.58 (4H, t, *J* = 8.0 Hz), 7.44 (4H, d, *J* = 8.0 Hz), 7.10 (4H, t, *J* = 6.0 Hz), 6.97 (2H, s), 6.80-6.74 (1H, m), 6.57 (1H, d, *J* = 7.6 Hz), 4.86 (1H, q, *J* = 13.2 Hz, 5.6 Hz), 3.84 (8H, s), 3.76 (4H, s), 3.65 (3H, s), 3.05 (2H, d, *J* = 6.0 Hz), 2.89 (2H, m), 2.14 (6H, s). ESI-TOF-MS *m/z* $[M + H]^+$ calcd for $C_{42}H_{49}N_8O_4$ 729.39; Found 729.40.

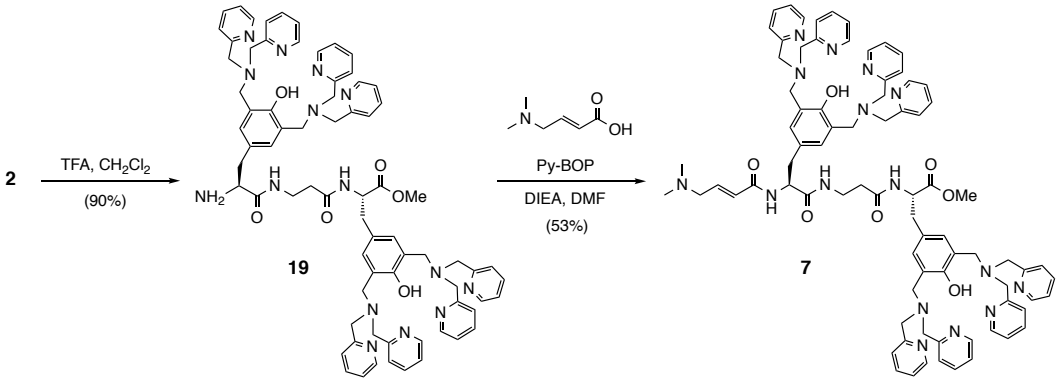

Synthesis of **19**

To an ice-cooled solution of **2** (300 mg, 0.24 mmol) in dry CH_2Cl_2 (2.0 mL) was added dropwise TFA (2.5 mL) and the solution was stirred for 1 h at rt. After removal of the solvent in vacuo, the residue was dissolved in H_2O. The mixture was neutralized with aqueous NH_3 on ice-cooling and then extracted with CH_2Cl_2. The organic layer was washed with brine followed by drying over Na_2SO_4. The solution was concentrated by evaporation to give **19** (250 mg, 90%) as a colorless amorphous powder.

^{1}H-NMR (400 MHz, $CDCl_3$) : δ 10.96 (2H, br), 8.50 (8H, t, *J* = 2.4 Hz), 7.76 (1H, m), 7.59 (8H, t, *J* = 7.6 Hz), 7.45 (8H, t, *J* = 8.0 Hz), 7.10 (8H, t, *J* = 6.0 Hz), 7.03 (2H, s), 6.97 (2H, s), 4.77 (1H, dd, *J* = 6.8 Hz), 3.84 (16H, s), 3.80-3.73 (9H, m), 3.62 (3H, s), 3.44-3.35 (4H, m), 3.11-2.98

(4H, m), 2.56-2.50 (1H, m), 2.25-2.24 (2H, m). ESI-TOF-MS *m/z* $[M + H]^+$ calcd for $C_{74}H_{80}N_{15}O_6$ 1274.64; Found 1274.66.

Synthesis of **7**

To an ice-cooled solution of 4-(dimethylamino)-2-butenoic acid hydrochloride (3.8 mg, 25 μmol) in dry DMF (1.0 mL) was added DIEA (12 μL, 63 μmol), Py-BOP (12 mg, 24 μmol) and **19** (20 mg, 16 μmol). The solution was stirred for 38 h at rt. After dilution with AcOEt, the solution was washed with saturated $NaHCO_3$ and brine followed by drying over Na_2SO_4. After removal of the solvent by evaporation, the residue was purified by column chromatography on SiO_2 ($CHCl_3$: MeOH : NH_3 = 400 : 4 : 1→180 : 30 : 1) to give **7** (12 mg, 53%) as a colorless oil. ^{1}H-NMR (400 MHz, DMSO-d_6) : δ 10.93 (1H, s), 10.81 (1H, s), 8.45 (8H, d, *J* = 4.8 Hz), 8.30 (1H, d, *J* = 9.2 Hz), 8.12 (1H, d, *J* = 8.4 Hz), 7.98 (1H, m), 7.68 (8H, t, *J* = 7.2 Hz), 7.42 (8H, d, *J* = 7.6 Hz), 7.20 (8H, dd, *J* = 1.4 Hz, 6.2 Hz), 7.03 (2H, s), 6.99 (2H, s), 6.36-6.33 (1H, m), 5.96 (1H, d, *J* = 15.6 Hz), 4.50-4.40 (2H, m), 3.71 (16H, d, *J* = 8.4 Hz), 3.61 (8H, d, *J* = 11.2 Hz), 3.42 (3H, s), 3.15-3.14 (4H, m), 2.88-2.62 (8H, m), 2.24-2.14 (4H, m), 1.93 (6H, s). ESI-TOF-MS *m/z* $[M + H]^+$ calcd for $C_{80}H_{19}N_{16}O_7$ 1385.71; Found 1385.72.

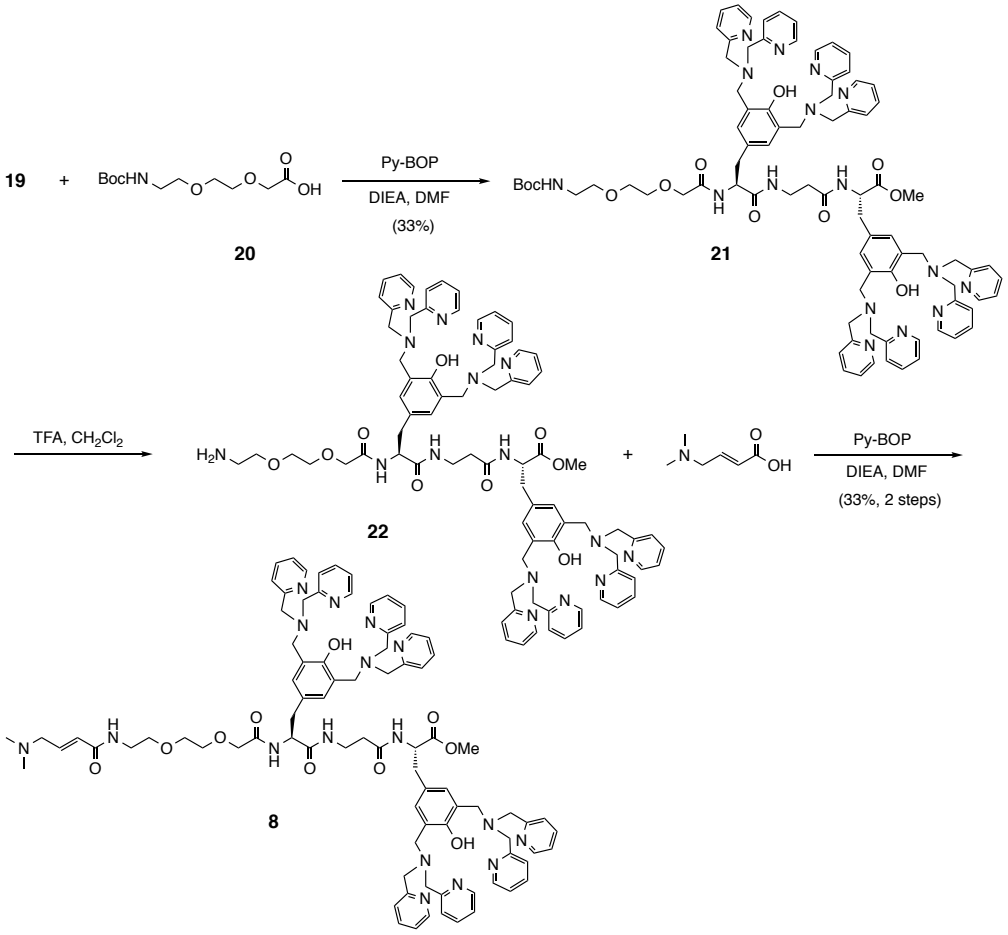

Synthesis of **21**

To an ice-cooled solution of **20** (13 mg, 47 μmol) in dry DMF (1.5 mL) was added DIEA (23 μL, 126 μmol), Py-BOP (25 mg, 47 μmol) and **19** (40 mg, 31 μmol) and the solution was stirred for 13 h at rt. After dilution with AcOEt, the solution was washed with saturated $NaHCO_3$ and brine followed by drying over Na_2SO_4. After removal of the solvent by evaporation, the residue was purified by column chromatography on SiO_2 ($CHCl_3$: MeOH : NH_3 = 400 : 4 : 1→160 : 20 : 1) to give **21** (44 mg, 33%) as a colorless oil. This material contained a small amount of impurities but was used for the next reaction without further purification.

^{1}H-NMR (400 MHz, DMSO-d_6) : δ 10.93 (1H, s), 10.87 (1H, s), 8.45 (8H, d, J = 3.6 Hz), 8.31 (1H, d, J = 7.6 Hz), 8.06 (1H, t), 7.68 (8H, t, J = 7.6 Hz), 7.50 (1H, d, J = 8.0 Hz), 7.42 (8H, d, J = 7.6 Hz), 7.20 (8H, dd, J = 1.6 Hz, 6.0 Hz), 6.98 (4H, d, J = 2.4 Hz), 6.73 (1H, t), 4.51-4.39 (2H, m), 3.73 (16H, s), 3.63 (8H, d, J = 2.8 Hz), 3.42 (3H, s), 3.15 (4H, m), 2.89-2.66 (6H, m), 2.31-2.07 (4H, m), 1.32 (9H, s). ESI-TOF-MS *m/z* $[M + H]^+$ calcd for $C_{85}H_{96}N_{16}O_{11}$ 1520.77; Found 1520.78.

Synthesis of **22**

To an ice-cooled solution of the crude **21** (43 mg) in CH_2Cl_2 (1 mL) was added dropwise TFA (1 mL) and the solution was stirred for 1 h at rt. After removal of the solvent in vacuo, the residue was dissolved in H_2O. The mixture was neutralized with aq. NH_3 on ice-cooling and extracted with CH_2Cl_2 (x2). The organic layer was washed with brine followed by drying over Na_2SO_4. The solution was concentrated by evaporation to give **22** (41 mg, quant) as a colorless oil. This material contained a small amount of impurities but was used for the next reaction without further purification.

^{1}H-NMR (400 MHz, $CDCl_3$) : δ 11.03 (2H, br), 8.49 (8H, t, *J* = 5.6 Hz), 7.58 (8H, dd, *J* = 8.0 Hz, 11.6 Hz), 7.42 (8H, t, *J* = 7.2 Hz), 7.37 (1H, t, *J* = 7.2 Hz), 7.12-7.08 (8H, m), 7.02 (2H, s), 6.98 (2H, s), 4.64-4-57 (2H, m), 3.83 (16H, s), 3.77-3.71 (8H, m), 3.56 (3H, s), 3.55-3.46 (6H, m), 3.10-2.82 (8H, m), 2.20-2.04 (4H, m). ESI-TOF-MS *m/z* $[M + H]^+$ calcd for $C_{80}H_{91}N_{16}O_9$ 1419.71; Found 1419.73.

Synthesis of **8**

To an ice-cooled solution of 4-(dimethylamino)-2-butenoic acid hydrochloride (3.4 mg, 21 μmol) in dry DMF (1 mL) was added DIEA (10 μL, 56 μmol), Py-BOP (11 mg, 21 μmol) and the crude **22** (20 mg). The solution was stirred for 14.5 h at rt. After dilution with AcOEt, the solution was washed with saturated $NaHCO_3$ and brine followed by drying over Na_2SO_4. After removal of the solvent by evaporation, the residue was purified by column chromatography on SiO_2 ($CHCl_3$: MeOH : NH_3 = 400 : 4 : 1→200 : 4 : 1→180 : 30 : 1) to give **8** (7 mg, 33%) as a colorless oil.

^{1}H-NMR (400 MHz, DMSO-d_6) : δ 10.93 (1H, s), 10.88 (1H, s), 8.46 (8H, d, *J* = 3.6 Hz), 8.46 (8H, d, *J* = 3.6 Hz), 8.36 (1H, m), 8.20 (1H, m), 8.02 (1H, m), 7.68 (8H, t, *J* = 7.2 Hz), 7.52 (1H, d), 7.41 (8H, d, *J* = 8.0 Hz), 7.20 (8H, d, *J* = 7.6 Hz), 6.98 (4H, s), 6.52 (1H, m), 6.06 (1H, m), 4.56-4.38 (4H, m), 3.72-3.63 (26H, m), 3.42 (3H, s), 3.15 (4H, m), 2.90 (6H, m), 2.30-2.11 (4H, m), 2.06 (6H, s). ESI-TOF-MS *m/z* $[M + H]^+$ calcd for $C_{86}H_{100}N_{17}O_{10}$ 1530.78; Found 1530.78.

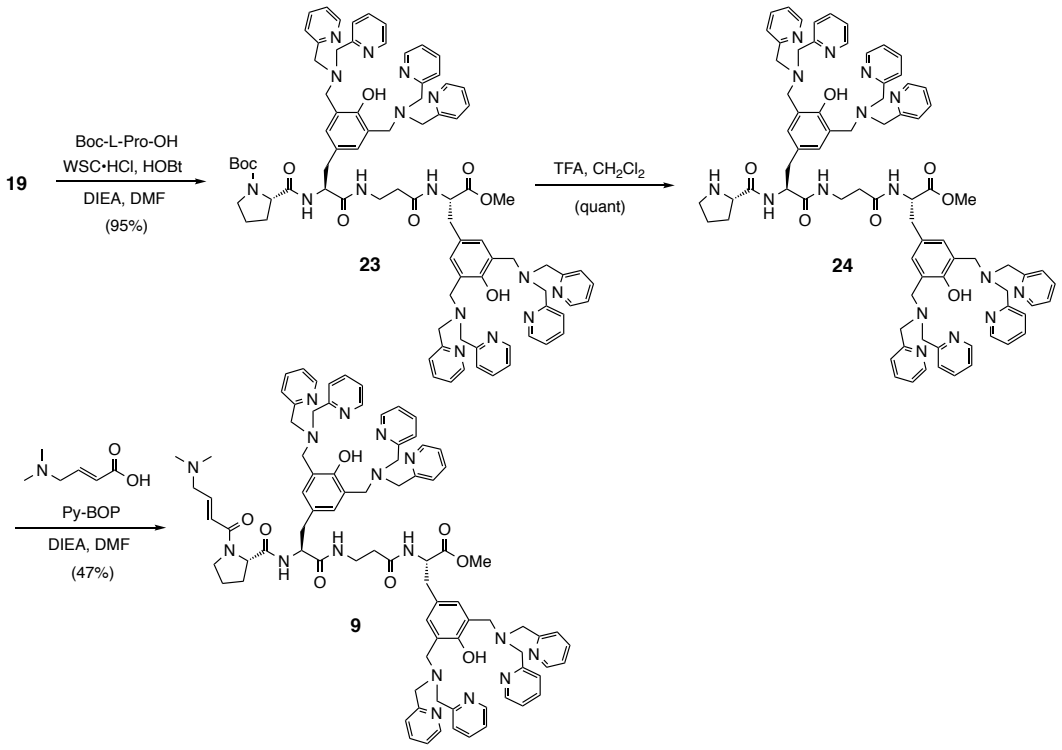

Synthesis of **23**

To an ice-cooled solution of **19** (20 mg, 16 μmol) in dry DMF (1.0 mL) was added WSCI•HCl (3.6 mg, 19 μmol), HOBt•H_2O (2.9 mg, 19 μmol), DIEA (12 μL, 75 μmol) and Boc-L-Pro (4 mg, 19 μmol). The solution was stirred for 13 h at rt. After dilution with AcOEt, the solution was washed with saturated $NaHCO_3$ and brine followed by drying over Na_2SO_4. After removal of the solvent by evaporation, the residue was purified by column chromatography on SiO_2 ($CHCl_3$: MeOH : NH_3 = 400 : 4 : 1→160 : 20 : 1) to give **23** (22 mg, 95%) as a colorless amorphous powder.

^{1}H-NMR (400 MHz, $CDCl_3$) : δ 10.98 (2H, br), 8.49 (8H, d, *J* = 4.0 Hz), 7.58 (8H, dd, *J* = 8.0 Hz, 11.6 Hz), 7.45 (8H, t, *J* = 6.8 Hz), 7.12-7.08 (8H, m), 6.99 (4H, s), 6.77 (2H, m), 4.68-4.53 (2H, m), 4.11 (1H, m), 3.83-3.75 (24H, m), 3.57 (3H, s), 3.20-2.96 (10H, m), 2.22 (4H, m), 1.62 (9H, br). ESI-TOF-MS *m/z* $[M + H]^+$ calcd for $C_{84}H_{95}N_{16}O_9$ 1472.75; Found 1472.75.

Synthesis of **24**

To an ice-cooled solution of **23** (20 mg, 13.6μmol) in CH_2Cl_2 (1 mL) was added dropwise TFA (1 mL) and the solution was stirred for 1 h at rt. After removal of the solvent in vacuo, the residue was dissolved in H_2O. The mixture was neutralized with aq. NH_3 on ice-cooling and extracted

with CH_2Cl_2. The organic layer was washed with brine followed by drying over Na_2SO_4. The solution was concentrated by evaporation to give **24** (24 mg, quant) as a colorless oil.

^{1}H-NMR (400 MHz, $CDCl_3$) : δ 10.95 (2H, br), 8.49 (8H, t, *J* = 3.2 Hz), 8.02 (1H, m), 7.58 (8H, dd, *J* = 7.2 Hz, 10.4 Hz), 7.45 (8H, t, *J* = 8.8 Hz), 7.37 (1H, t, *J* = 8.0 Hz), 7.10-7.02 (8H, m), 7.00 (5H, s), 4.63 (2H, dd, *J* = 5.2 Hz), 4.41 (2H, m), 4.11 (1H, m), 3.87-3.75 (24H, m), 3.60 (3H, s), 3.22-2.10(14H, m). ESI-TOF-MS *m/z* $[M + H]^+$ calcd for $C_{79}H_{87}N_{16}O_7$ 1371.69; Found 1371.70.

Synthesis of **9**

To an ice-cooled solution of 4-(dimethylamino)-2-butenoic acid hydrochloride (3.4 mg, 21 μmol) in dry DMF (1 mL) was added a mixture of DIEA (10 μL, 56 μmol), Py-BOP (11 mg, 21 μmol) and **24** (22 mg, 14 μmol). The solution was stirred for 18 h at rt. After dilution with AcOEt, the solution was washed with saturated $NaHCO_3$ and brine followed by drying over Na_2SO_4. After removal of the solvent by evaporation, the residue was purified by column chromatography on SiO_2 ($CHCl_3$: MeOH : NH_3 = 400 : 4 : 1→160 : 20 : 1) to give **9** (11 mg, 47%) as a colorless amorphous powder.

^{1}H-NMR (400 MHz, DMSO-d_6) : δ 10.94 (2H, d), 8.46 (8H, d), 8.30 (1H, d, *J* = 10 Hz), 7.79 (1H, m), 7.68 (8H, t, *J* = 7.6 Hz), 7.44 (8H, t, *J* = 8.0 Hz), 7.21 (8H, t, *J* = 5.6 Hz), 6.99 (4H, s), 6.58 (1H, m), 6.32 (1H, m), 4.41 (2H, m), 3.72 (16H, s), 3.64 (8H, s), 3.42 (3H, s), 3.18-2.78 (12H, m), 2.12 (6H, br), 1.87 (2H, m). ESI-TOF-MS *m/z* $[M + H]^+$ calcd for $C_{85}H_{96}N_{17}O_8$ 1482.76; Found 1482.76.

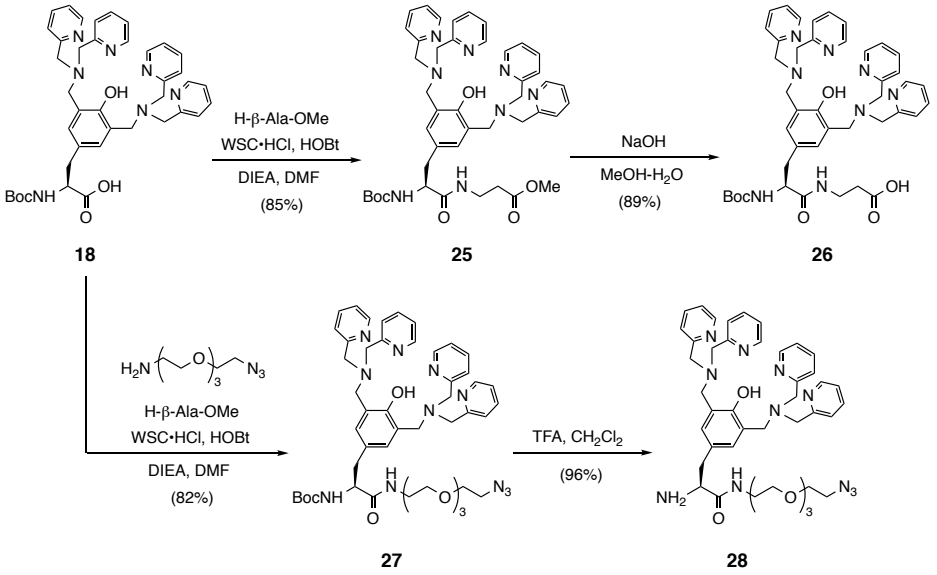

Synthesis of **25**

To an ice-cooled solution of **18** (1.0 g, 1.42 mmol) in dry DMF (6 mL) was added WSCI•HCl (355 mg, 1.85 mmol), HOBt•H_2O (283 mg, 1.85 mmol), DIEA (0.9 mL, 5.68 mmol) and H-□□la-OMe•HCl (258 mg, 1.85 mmol). The solution was stirred for 6 h at rt. After dilution with AcOEt, the solution was washed with saturated $NaHCO_3$ and brine followed by drying over Na_2SO_4. After removal of the solvent by evaporation, the residue was purified by column chromatography on SiO_2 ($CHCl_3$: MeOH : NH_3 = 300 : 10 : 1 → 200 : 10 : 1) to give **25** (953 mg, 85%) as a colorless amorphous powder.

^{1}H-NMR(400 MHz, $CDCl_3$): δ 10.98 (1H, br), 8.54 (4H, d, J = 4.8 Hz), 7.60 (4H, t, J = 6.8 Hz), 7.45 (4H, d, J = 8.0 Hz), 7.12 (4H, t, J = 8.0 Hz), 7.04 (2H, s), 5.32 (1H, m), 4.30 (1H, m), 3.90-3.70 (12H, m), 3.46 (3H, s), 3.31-3.23 (2H, m), 3.02-2.97 (1H, m), 2.87-2.81 (1H, m), 2.34-2.17 (2H, m), 1.36 (9H, s). ESI-TOF-MS *m/z* $[M + H]^+$ calcd for $C_{44}H_{53}N_8O_6$ 789.41; Found 789.41.

Synthesis of **26**

To an ice-cooled solution of **25** (916 mg, 1.16 mmol) in MeOH-H_2O (18 : 5 (v/v), 23 mL) was added 5 N NaOH (696 □L, 3.48 mmol) and the solution was stirred for 7 h at 0 ˚C. After dilution with water, the solution was washed with diethyl ether (x2). The pH was adjusted to 5 and extracted with $CHCl_3$ (x2). The organic phase was dried over Na_2SO_4 and concentrated in vacuo. The residue was washed with hexane-*i*-PrOH (1 : 1) to give **26** (804 mg, 89%) as a colorless amorphous powder.

^{1}H-NMR (400 MHz, $CDCl_3$) : δ 8.54 (4H, m), 7.70-7.52 (8H, m), 7.13 (4H, m), 7.01 (2H, s), 6.70 (1H, m), 5.55 (1H, m), 4.37 (1H, m), 4.00 (12H, m), 3.46 (1H, m), 3.26 (1H, m), 3.09-3.07 (1H,

m), 2.76-2.70 (1H, m), 2.22 (2H, m). ESI-TOF-MS *m/z* $[M + H]^+$ calcd for $C_{43}H_{51}N_8O_6$ 775.39; Found 775.38.

Synthesis of **27**

To an ice-cooled solution of **18** (200 mg, 0.28 mmol) in dry DMF (3.0 mL) was added WSCI•HCl (83 mg, 0.43 mmol), HOBt•H_2O (64 mg, 0.43 mmol), DIEA (148 μL, 0.85 mmol) and 11-azido-3,6,9-trioxaundecan-1-amine (56 μL, 0.28 mmol). The solution was stirred overnight at rt. After dilution with AcOEt, the solution was washed with saturated $NaHCO_3$ and brine followed by drying over Na_2SO_4. After removal of the solvent by evaporation, the residue was purified by column chromatography on SiO_2 ($CHCl_3$: MeOH : NH_3 = 400 : 10 : 1 → 300 : 10 : 1) to give **27** (211 mg, 82%) as a colorless oil.

^{1}H-NMR(400 MHz, $CDCl_3$): δ 10.97 (1H, br), 8.53 (4H, d, *J* = 3.6 Hz), 7.60 (4H, t, *J* = 7.6 Hz), 7.45 (4H, d, *J* = 8.0 Hz), 7.12 (4H, t, *J* = 7.6 Hz), 7.05 (2H, s), 6.90 (1H, br), 4.33 (1H, m), 3.85 (8H, s), 3.75 (4H, dd, *J* = 19.2 Hz, 14 Hz), 3.66-3.24 (19H, m), 3.00-2.86 (2H, m), 1.35 (9H, s). ESI-TOF-MS *m/z* $[M + H]^+$ calcd for $C_{48}H_{62}N_{11}O_7$ 904.48; Found 904.50.

Synthesis of **28**

To an ice-cooled solution of **27** (210 mg, 232 μmol) in CH_2Cl_2 (1.5 mL) was added dropwise TFA (1.5 mL) and the solution was stirred for 1 h at rt. After removal of the solvent in vacuo, the residue was dissolved in H_2O. The mixture was neutralized with aq. NH_3 on ice-cooling, diluted with saturated $NaHCO_3$, and then extracted with CH_2Cl_2 (x2). The organic layer was dried over Na_2SO_4. The solution was concentrated by evaporation to give **28** (176 mg, 96%) as a pale yellow oil.

^{1}H-NMR (400 MHz, $CDCl_3$) : δ 10.99 (1H, br), 8.51 (4H, d, *J* = 4.8 Hz), 7.63-7.59 (4H, m), 7.47 (4H, d, *J* = 8.0 Hz), 7.11 (4H, t, *J* = 6.4 Hz), 7.05 (2H, s), 3.86 (8H, s), 3.80 (4H, s), 3.69-3.34 (16H, m), 3.18-3.14 (2H, m), 2.58-2.51 (1H, m). ESI-TOF-MS *m/z* $[M + H]^+$ calcd for $C_{43}H_{54}N_{11}O_5$ 804.43; Found 804.44.

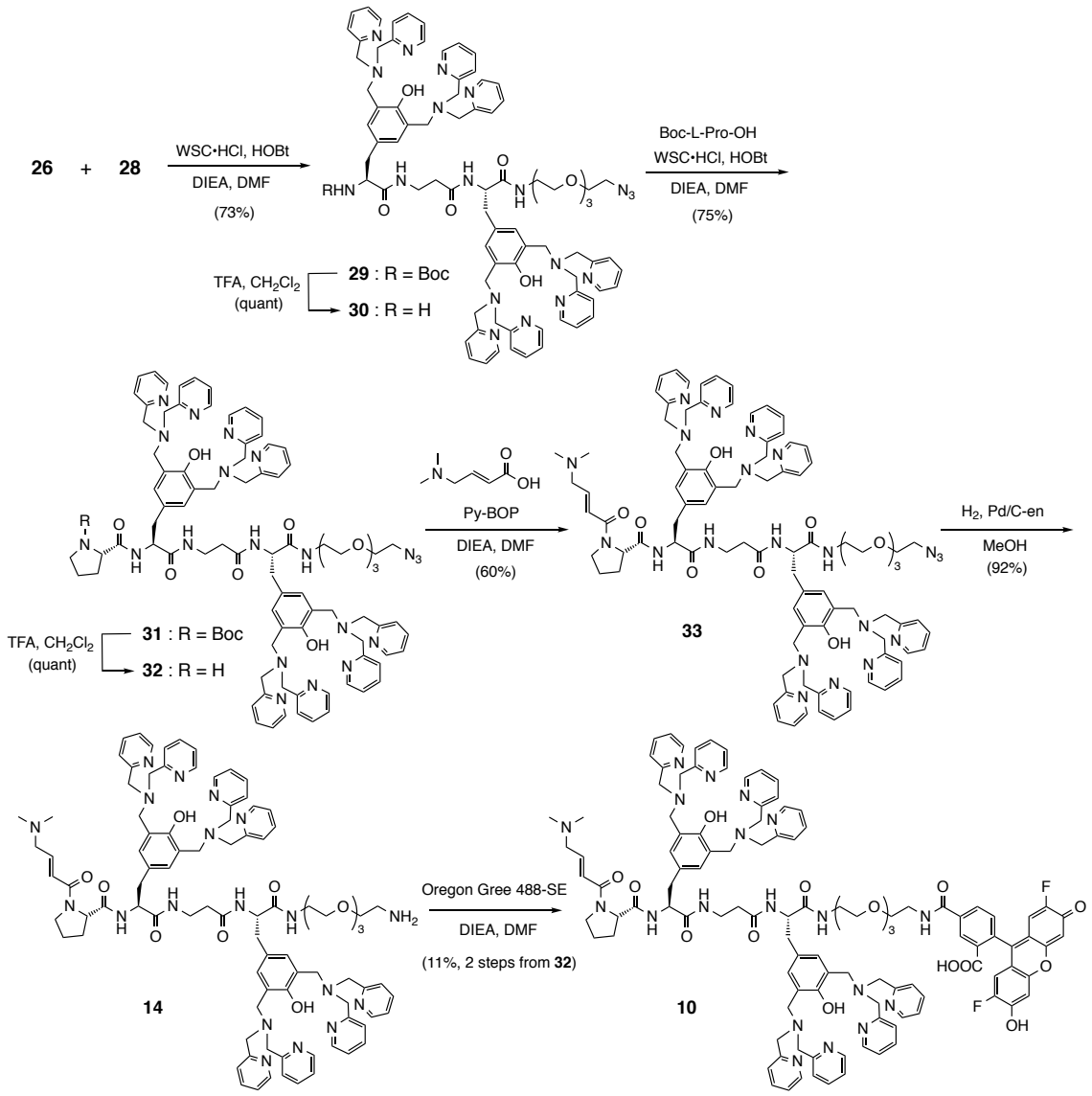

Synthesis of **29**

To a solution of **28** (99 mg, 132 μmol) in dry DMF (2 mL) was added WSCI•HCl (36 mg, 185 μmol), HOBt•H_2O (28 mg, 185 μmol), DIEA (86 μL, 492 μmol) and **26** (115 mg, 148 μmol). The solution was stirred overnight at rt. After dilution with AcOEt, the solution was washed with saturated $NaHCO_3$ and brine followed by drying over Na_2SO_4. After removal of the solvent by evaporation, the residue was purified by column chromatography on SiO_2 ($CHCl_3$: MeOH : NH_3 = 200 : 10 : 1) to give **29** (140 mg, 73%) as a colorless amorphous powder.

^{1}H-NMR (400 MHz, $CDCl_3$) : δ 10.99 (2H, br), 8.54-8.51 (8H, m), 7.61-7.58 (8H, m), 7.52-7.43 (8H, m), 7.14-7.02 (12H, m), 5.44 (1H, m), 4.62-4.60 (1H, m), 4.29 (1H, m), 3.84-3.18 (42H, m),

2.95-2.85 (6H, m), 2.27-2.17 (2H, m), 1.27 (9H, s). ESI-TOF-MS 1561.78 $[M + H]^+$. ESI-TOF-MS *m/z* $[M + H]^+$ calcd for $C_{86}H_{102}N_{19}O_{10}$ 1561.88; Found 1561.78.

Synthesis of **30**

To an ice-cooled solution of **29** (139 mg, 89 μmol) in CH_2Cl_2 (2 mL) was added dropwise TFA (2 mL) and the solution was stirred for 2 h at rt. After removal of the solvent in vacuo, the residue was dissolved in H_2O. The mixture was neutralized with aq. NH_3 on ice-cooling, diluted with saturated $NaHCO_3$, and then extracted with CH_2Cl_2. The organic layer was dried over Na_2SO_4. The solution was concentrated by evaporation to give **30** (130 mg, quant) as a pale red amorphous powder.

^{1}H-NMR (400 MHz, $CDCl_3$) : δ 10.99 (2H, br), 8.50 (8H, dd, *J* = 7.6 Hz, 4.0 Hz), 7.62-7.57 (8H, m), 7.48-7.43 (8H, t, *J* = 8.8 Hz), 7.14-7.02 (12H, m), 4.66 (1H, m), 3.84-3.06 (46H, m), 2.96-2.86 (2H, m), 2.31 (2H, m). ESI-TOF-MS *m/z* $[M + H]^+$ calcd for $C_{81}H_{94}N_{19}O_8$ 1460.75; Found 1460.76.

Synthesis of **31**

To an ice-cooled solution of **30** (40 mg, 27 μmol) in dry DMF (1.5 mL) was added WSCI•HCl (6.4 mg, 33 μmol), HOBt•H_2O (5 mg, 25 μmol), DIEA (22 μL, 132 μmol) and Boc-L-Pro (7 mg, 33 μmol). The solution was stirred for 4.5 h at rt. After dilution with AcOEt, the solution was washed with saturated $NaHCO_3$ and brine followed by drying over Na_2SO_4. After removal of the solvent by evaporation, the residue was purified by column chromatography on SiO_2 ($CHCl_3$: MeOH : NH_3 = 400 : 4 : 1 → 160 : 20 : 1) to give **31** (34 mg, 75%) as a pale yellow oil.

^{1}H-NMR (400 MHz, $CDCl_3$) : δ 10.95-10.94 (2H, m), 8.52 (8H, t, *J* = 4.0 Hz), 7.58 (8H, t, *J* = 7.6 Hz), 7.44 (8H, t, *J* = 6.8 Hz), 7.32 (1H, m), 7.13-7.11 (8H, t, *J* = 5.2 Hz), 7.02-7.00 (3H, m), 6.72 (1H, m), 4.60-4.52 (2H, m), 4.11 (1H, m), 3.83 (16H, s), 3.71-3.18 (28H, m), 2.90-2.89 (3H, m), 2.25 (1H, m), 1.93 (2H, m), 1.71 (13H, m). ESI-TOF-MS *m/z* $[M + H]^+$ calcd for $C_{91}H_{109}N_{20}O_{11}$ 1658.86; Found 1658.89.

Synthesis of **32**

To an ice-cooled solution of **31** (32 mg, 19 μmol) in dry CH_2Cl_2 (1.0 mL) was added dropwise TFA (1.0 mL) and the solution was stirred for 1 h at rt. After removal of the solvent in vacuo, the residue was dissolved in H_2O. The mixture was neutralized with aq. NH_3 on ice-cooling, diluted with saturated $NaHCO_3$, and then extracted with CH_2Cl_2 (x2). The organic layer was washed with

brine and dried over Na_2SO_4. The solution was concentrated by evaporation to give **32** (32 mg, quant) as a colorless oil.

^{1}H-NMR (400 MHz, $CDCl_3$) : δ 10.95 (2H, brs), 8.51 (8H, t, *J* = 5.2 Hz), 8.04 (1H, m), 7.58 (8H, t, *J* = 8.0 Hz), 7.43 (8H, t, *J* = 8.0 Hz), 7.14-7.10 (8H, m), 7.04 (4H, s), 4.57-4.47 (2H, m), 3.83 (16H, s), 3.80-2.52 (31H, m), 2.27-1.66(7H, m). ESI-TOF-MS *m/z* $[M + H]^+$ calcd for $C_{86}H_{101}N_{20}O_9$ 1558.81; Found 1558.84.

Synthesis of **33**

To an ice-cooled solution of 4-(dimethylamino)-2-butenoic acid hydrochloride (7.0 mg, 43 μmol) in dry DMF (1 mL) was added DIEA (19 μL, 116 μmol), Py-BOP (22 mg, 43 μmol) and **32** (30 mg, 19 μmol). The solution was stirred overnight at rt. After dilution with water, the solution was washed with saturated $NaHCO_3$ and brine followed by drying over Na_2SO_4. After removal of the solvent by evaporation, the residue was purified by column chromatography on SiO_2 ($CHCl_3$: MeOH : NH_3 = 400 : 4 : 1→160 : 20 : 1) to give **33** (19 mg, 60%) as a colorless oil.

^{1}H-NMR (400 MHz, $CDCl_3$) : δ 10.95 (2H, br), 8.50 (8H, dd, *J* = 11.2 Hz, 4.4 Hz), 7.58 (8H, t, *J* = 7.6 Hz), 7.43 (8H, t, *J* = 8.4 Hz), 7.34-7.32 (2H, m), 7.13-7.09 (8H, m), 7.01 (4H, d, *J* = 5.2 Hz), 6.80-6.74 (1H, m), 4.60-4.58 (1H, m), 4.38 (2H, m), 3.83 (16H, s), 3.79-3.01 (28H, m), 2.88-2.84 (2H, m), 2.39-2.35 (1H, m), 2.21 (8H, br), 1.75 (4H, m). ESI-TOF-MS *m/z* $[M + H]^+$ calcd for $C_{92}H_{110}N_{21}O_{10}$ 1669.88; Found 1669.91.

Synthesis of **14**

A solution of **33** (18 mg, 11μmol) and Pd/C-ethylenediamine complex (10 mg) in MeOH-CH_2Cl_2 (1 : 1, 5 mL) was vigorously stirred for 5 h under H_2 atmosphere at rt. After filtration, the solvent was removed by evaporation to give the crude **14** (20 mg) as a pale yellow oil. This material used for the next reaction without further purification.

ESI-TOF-MS *m/z* $[M + H]^+$ calcd for $C_{92}H_{112}N_{19}O_{10}$ 1642.88; Found 1642.91.

Synthesis of **10**

A mixture of crude **14** (10 mg), DIEA (18 μL, 108 μmol), Oregon Green 488-SE (2.5 mg, 5 μmol) in dry DMF (2 mL) was stirred for 3 h at rt. The reaction was monitored by reverse-phase HPLC. Purification by reverse-phase HPLC and subsequent lyophilization gave **10** (2.4 mg, 11%

in two steps) as a yellow powder. The purity of **10** was determined to be > 95% by HPLC analysis (UV, λ = 220 nm).

HPLC conditions: column; YMC-pack ODS-A, 250 x 20 mm, mobile phase; CH_3CN (containing 0.1% TFA) / H_2O (containing 0.1% TFA) = 5 / 95 (10 min) → 50 / 50 (linear gradient over 50 min), flow rate; 9.9 mL/min, detection; UV (λ = 220 nm).

ESI-TOF-MS *m/z* $[M + H]^+$ calcd for $C_{113}H_{120}F_2N_{19}O_{16}$ 2037.92; Found 2037.91.

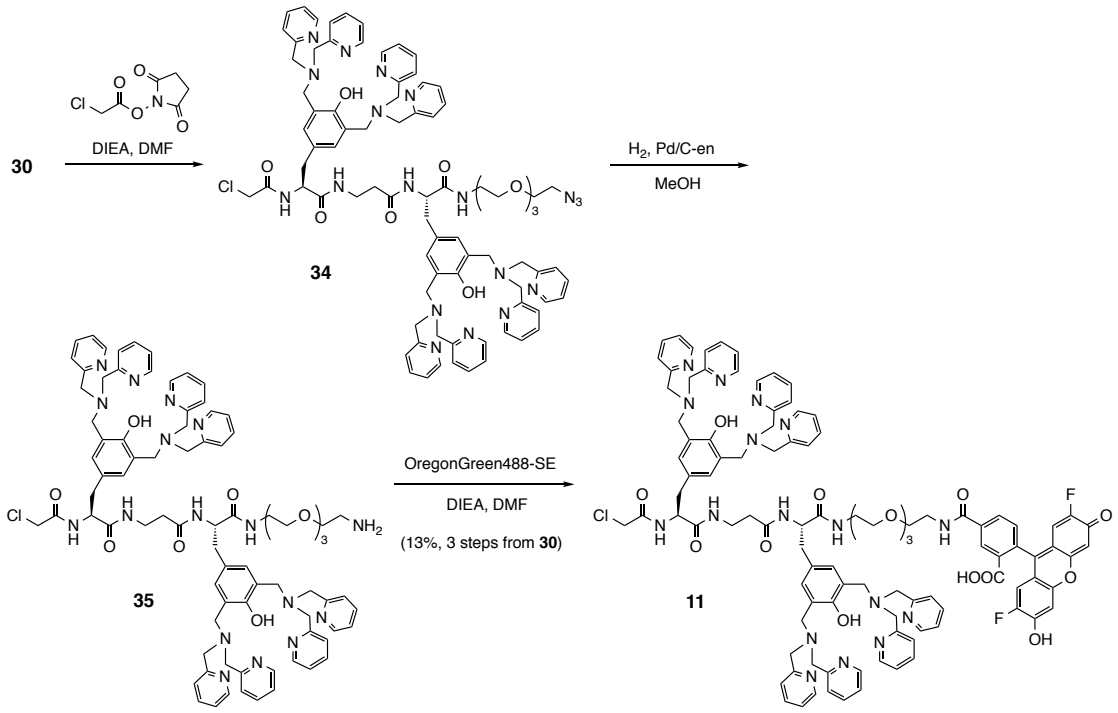

Synthesis of **34**

To a solution of **30** (20 mg, 14 μmol) in dry DMF (1.0 mL) was added DIEA (7 μL, 41 μmol) and chloroacetic acid *N*-hydroxysuccinimidyl ester (4.0 mg, 19 μmol) and the solution was stirred for 2 h at rt. After dilution with AcOEt, the solution was washed with saturated $NaHCO_3$ and brine followed by drying over Na_2SO_4. The solvent was removed by evaporation to give crude **34** (21 mg) as a pale yellow oil. This material used for the next reaction without further purification.

ESI-TOF-MS *m/z* $[M + H]^+$ calcd for $C_{83}H_{95}ClN_{19}O_9$ 1536.72; Found 1536.72.

Synthesis of **35**

A solution of the crude **34** (21 mg) and Pd/C-ethylenediamine complex (10 mg) in MeOH-CH_2Cl_2 (1 : 1, 5 mL) was vigorously stirred for 5 h under H_2 atmosphere at rt. After filtration, the solvent was removed by evaporation to give crude **35** (17 mg) as a pale yellow oil. This material used for the next reaction without further purification.

ESI-TOF-MS *m/z* $[M + H]^+$ calcd for $C_{83}H_{97}ClN_{17}O_9$ 1510.73; Found 1510.74.

Synthesis of **11**

A mixture of the crude **35** (17 mg), DIEA (18 μL, 108 μmol), Oregon Green 488-SE (2.5 mg, 5 μmol) in dry DMF (1.5 mL) was stirred for 3 h at rt. The reaction was monitored by reverse-phase HPLC. Purification by reverse-phase HPLC and lyophilization gave **11** (3.3 mg, 13% in three steps) as a yellow powder. The purity of **11** was determined to be > 95% by HPLC analysis (UV, λ = 220 nm).

HPLC conditions: column; YMC-pack ODS-A, 250 x 20 mm, mobile phase; CH_3CN (containing 0.1% TFA) / H_2O (containing 0.1% TFA) = 0 / 100 → 50 / 50 (linear gradient over 50 min), flow rate; 9.9 mL/min, detection; UV (λ = 220 nm).

ESI-TOF-MS *m/z* $[M + H]^+$ calcd for $C_{104}H_{105}ClF_2N_{17}O_{15}$ 1905.77; Found 1905.76.

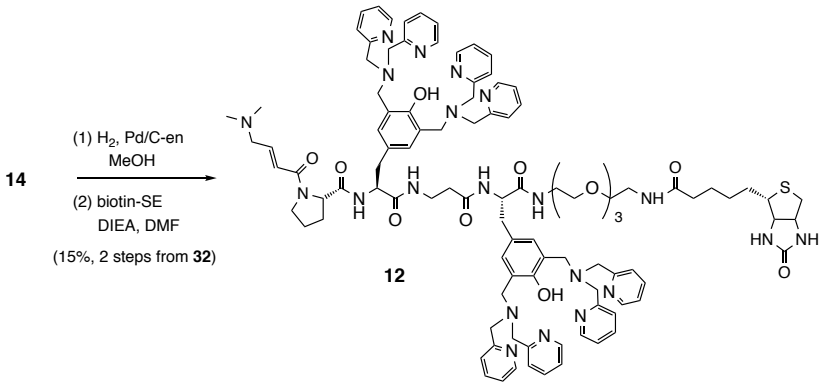

Synthesis of **12**

A mixture of crude **14** (7.1 mg), DIEA (10 μL, 58 μmol), biotin-SE (9.0 mg, 26 μmol) in dry DMF (1 mL) was stirred for 13 h at rt. The reaction was monitored by reverse-phase HPLC. Purification by reverse-phase HPLC and lyophilization gave **12** (2.0 mg, 15% in two steps) as a colorless powder. The purity of **12** was determined to be > 95% by HPLC analysis (UV, λ = 220 nm).

HPLC conditions: column; YMC-pack ODS-A, 250 x 10 mm, mobile phase; CH_3CN (containing 0.1% TFA) / H_2O (containing 0.1% TFA) = 5 / 95 (10 min) → 45 / 55 (linear gradient over 40 min), flow rate; 3.0 mL/min, detection; UV (λ = 220 nm).

ESI-TOF-MS *m/z* $[M + H]^{3+}$ calcd for $C_{102}H_{126}N_{21}O_{12}S$ 623.32; Found 624.33.

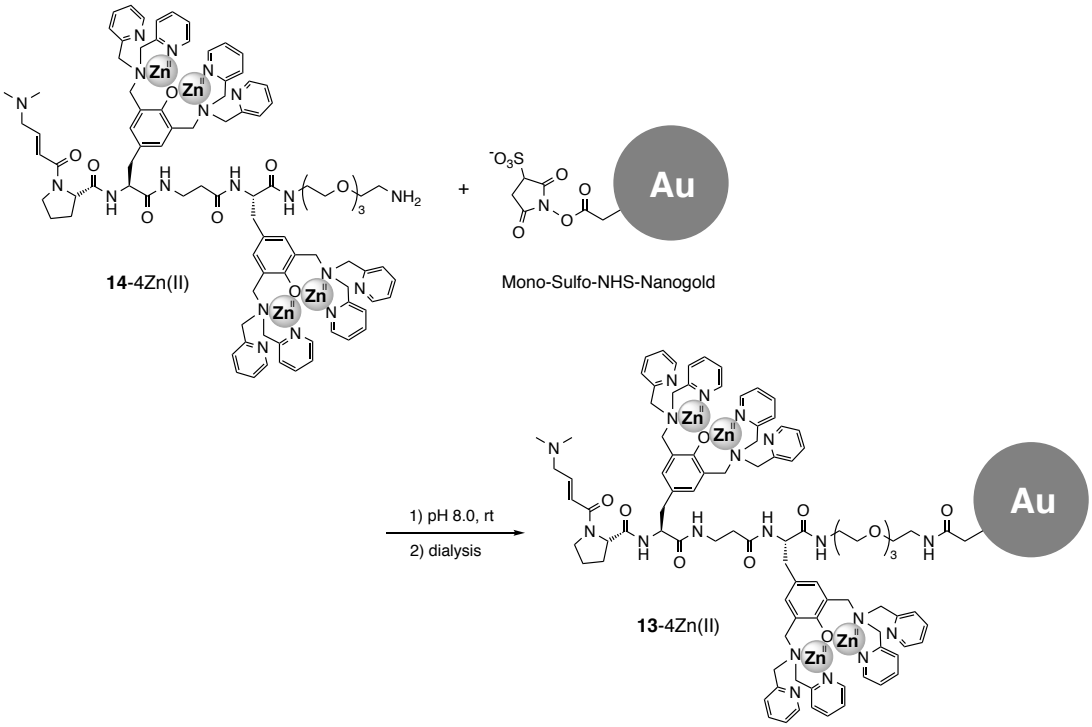

Synthesis of 13-4Zn(II)

Mono-Sulfo-NHS-Nanogold (purchased from Nanoprobes) (6 nmol) was dissolved in MilliQ water (200 μL) and mixed with the solution (200 μL) of the zinc complex **14**-4Zn(II) (~ 120 mmol) in 50 mM HEPES (pH 8.0), in which concentration of **14**-4Zn(II) was determined by UV absorbance at 280 nm using the measured extinction coefficient ($\varepsilon_{280\ nm}$ = 5170 $cm^{-1}M^{-1}$). The mixture was incubated at rt for 3 h with gentle shaking. The mixture was transferred into a dialysis membrane (MWCO: 14,000) and dialyzed (1 h x 3) against 300 mL of 50 mM HEPES (pH 7.2) containing 50 μM $ZnCl_2$ at rt to remove the excess of **14**-4Zn(II). The conjugation of **14**-4Zn(II) with the nanogold was confirmed by UV absorbance measurement at 280 nm and 420 nm, in which the absorbance ratio ($A_{280\ nm}$ / $A_{420\ nm}$ = 2.77) of the nanogold and the extinction coefficient of **14**-4Zn(II) were used to estimate the labeling yield.

References

Yamamori S, Itakura M, Sugaya D, Katsumata O, Sakagami H, and Takahashi M. (2011). Differential expression of SNAP-25 family proteins in the mouse brain. *J. Comp. Neurol. 519*, 916-932.

Luján, R. *et al.* (2018). Differential association of $GABA_B$ receptors with their effector ion channels in Purkinje cells. *Brain Struct. Func. 223*, 1565-1587.

Miki, T., Kaufmann, .W. A., Malagon, G., Gomez, L., Tabuchi, K., Watanabe M., Shigemoto, R., and Marty, A. (2017). Numbers of presynaptic Ca^{2+} channel clusters match those of functionally defined vesicular docking sites in single central synapses. *Proceed. Natl. Acad. Sci. USA 114*, E5246-E5255.

Nonaka, H., Fujishima, S., Uchinomiya, S., Ojida, A., and Hamachi, I. (2010). Selective covalent labeling of Tag-fused GPCR proteins on live cell surface with a synthetic probe for their functional analysis. *J. Am. Chem. Soc.*, *132*, 9301-9309.